Spring 2017

Simulation of Laser Induced Thermal Damage in Nd:YVO4 Crystals.

Richie Nagi
San Jose State University

SIMULATION OF LASER INDUCED THERMAL DAMAGE IN Nd:YVO_4 CRYSTALS

A Thesis

Presented to

The Faculty of the Department of Physics and Astronomy

San José State University

In Partial Fulfillment

of the Requirements for the Degree

Master of Science

by

Richie Nagi

May 2017

The Designated Thesis Committee Approves the Thesis Titled

SIMULATION OF LASER INDUCED THERMAL DAMAGE IN Nd:YVO_4 CRYSTALS

by

Richie Nagi

APPROVED FOR THE DEPARTMENT OF PHYSICS AND ASTRONOMY

SAN JOSÉ STATE UNIVERSITY

May 2017

Dr. Peter Beyersdorf	Department of Physics and Astronomy
Dr. Ramendra Bahuguna	Department of Physics and Astronomy
Dr. Neil Switz	Department of Physics and Astronomy

ABSTRACT

SIMULATION OF LASER INDUCED THERMAL DAMAGE IN Nd:YVO_4 CRYSTALS

by Richie Nagi

Neodymium-doped yttrium orthovanadate (Nd:YVO_4) is a commonly used gain medium in Diode Pumped Solid State (DPSS) lasers, but high heat loading of Nd:YVO_4 at high pump powers ($\geq$ 5 W) leads to thermal distortions and crystal fracture, which limits the utility of Nd:YVO_4 for high power applications. In this thesis, a Nd:YVO_4 crystal suffered thermal damage during experiments for investigating the optical gain characteristics of the crystal. This thesis examines the thermal damage mechanisms in detail. Principally, laser induced melting, as well as laser induced thermal stress fracture were studied, all in the absence of stimulated emission in the crystal. The optical system for coupling the pump laser light into the crystal was first simulated in Zemax, an optical design software, and the simulations were then compared to the experimental coupling efficiency results, which were found to be in agreement. The simulations for the laser coupling system were then used in conjunction with LASCAD, a finite element analysis software, to obtain the temperatures inside the crystal, as a function of optical power coupled into the crystal. The temperature simulations were then compared to the experimental results, which were in excellent agreement, and the temperature simulations were then generalized to other crystal geometries and Nd doping levels. Zemax and LASCAD were also used to simulate the thermal stress in the crystal as a function of the coupled optical power, and the simulations were compared to experiments, both of which were found to be in agreement. The thermal stress simulations were then generalized to different crystal geometries and Nd doping levels as well.

ACKNOWLEDGEMENTS

First of all, I would like to thank my adviser, Dr. Peter Beyersdorf, for all of his guidance and assistance. It was a great honor to work with him.

I would also like to thank Brianna Conroy from the San José State University Physics and Astronomy Department, as well as Kyle Arakaki and Peter Kiesel from the Palo Alto Research Center (A Xerox Company), for their assistance with the experimental measurements in this thesis.

I would also like to acknowledge the contributions of the members of the Machine and Electronics Shops at the San José State University Physics and Astronomy Department, principally Thao Le, Minh Mai, and Jose Garcia, for their assistance with mechanical and electrical issues in the lab.

I would also like to extend my appreciation to Bertha Aguayo from the San José State University Physics and Astronomy Department, and Katrice Hernandez from the Graduate Admissions and Program Evaluations Department at San José State University, for their assistance with administrative issues.

Finally, I would like to thank my parents, Virender Nagi and Jagdish Nagi, for their encouragement and support throughout this adventure.

TABLE OF CONTENTS

CHAPTER

LIST OF FIGURES

Figure

CHAPTER 1

DIODE PUMPED SOLID STATE LASERS

1.1 Optical amplification

To understand the operation of a laser, it is essential to know the fundamental principles that govern the interaction of radiation with matter. Particle systems such as atoms, ions, and molecules can exist only in discrete energy states. A change from one energy state to another, in the case of a radiative transition, is associated with either the emission or the absorption of a photon. The frequency of the absorbed or emitted radiation is given by the Bohr's frequency relation

$$E_2 - E_1 = h\nu_{21} \tag{1.1}$$

where E_2 and E_1 are two discrete energy levels, ν_{21} is the frequency of the photon emitted or absorbed, and h is Plancks constant. An electromagnetic wave with a frequency ν_{21}, which corresponds to an energy gap of the system described by equation 1.1, can interact with the system. To the approximation required in this context, a laser gain medium can be considered an ensemble of many identical systems. At thermal equilibrium, the lower energy states in the medium are more heavily populated than the higher energy states, as given by the Maxwell-Boltzmann distribution

$$f(E) = Ae^{-kT} \tag{1.2}$$

where *f(E)* is the is the probability that the particle will have energy E, A is the normalization constant, and e^{-kT} is the probability of the particle occupying a given

energy state. An electromagnetic wave interacting with the laser system will raise the particles (atoms, molecules etc.) from lower to higher energy levels, and thereby experience absorption.

The operation of a laser requires that the particle (atoms, molecules etc.) distribution of a laser material be changed such that more particles (atoms, molecules etc.) populate one particular higher energy state rather than one particular lower energy state. This is achieved by an external pump source that supplies the energy required to transfer particles (atoms, molecules etc.) from lower energy levels to a higher ones. Figure 1.1 [1] summarizes the the fundamental principles governing the interaction of radiation with matter for a two level system. An electromagnetic wave of appropriate frequency, incident on the inverted laser

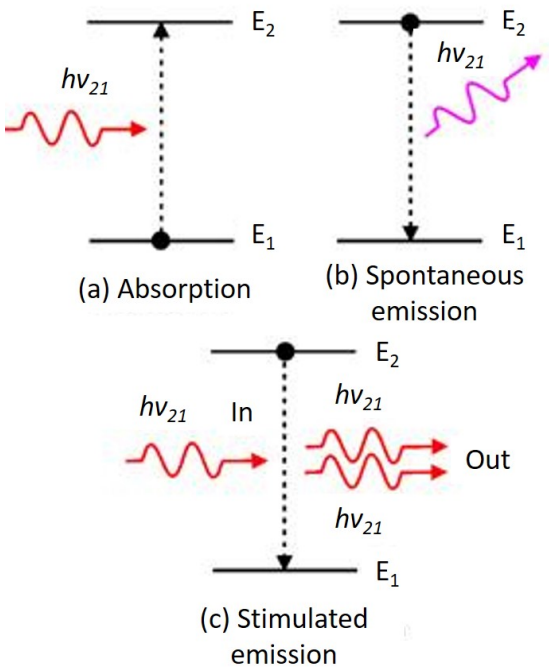

Figure 1.1: Types of atomic transitions for a two level system subjected to radiation. Adapted from [1].

material, will be amplified because the incident photons cause the particles (atoms,

molecules etc.) in the higher level to drop to a lower level and thereby emit additional photons. As a result, energy is extracted from the system and supplied to the radiation field.

Thus, when a material is excited in such a way as to provide more particles (atoms, molecules etc.) in a higher energy level than in some lower level, the material will be capable of amplifying radiation at the frequency corresponding to the energy level difference. Figure 1.2 [2] shows the energy level diagram of a typical 4-level laser. The fast decay mechanism shown in Figure 1.2 maximizes the population of level 2 while minimizing the population the population of level 1, thus maintaining a population inversion between levels 2 and 1. A detailed summary of the basics of laser physics can be found in [6], from which the above discussion was adapted.

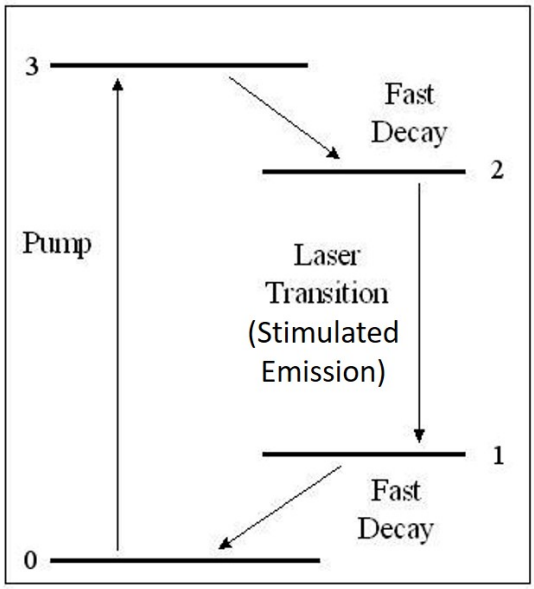

Figure 1.2: Four-level system. Adapted from [2].

1.1.1 Laser oscillators and amplifiers

Laser oscillators and amplifiers are crucial building blocks of high power diode pumped laser systems. Laser oscillators are the fundamental devices that generate laser radiation. Laser amplifiers, as the name suggests, amplify the light incident passing through the device. Common to all laser amplifiers and oscillators are at least two elements: a laser gain medium in which a population inversion among the particles (atoms, molecules etc.) can be achieved, and a pump process to supply energy to the system in order to build a population inversion. For a laser oscillator, a feedback mechanism is also required for the radiation to build up. For example, the laser oscillator shown in Figure 1.3 [3] has two mirrors facing each other that provide the required feedback.

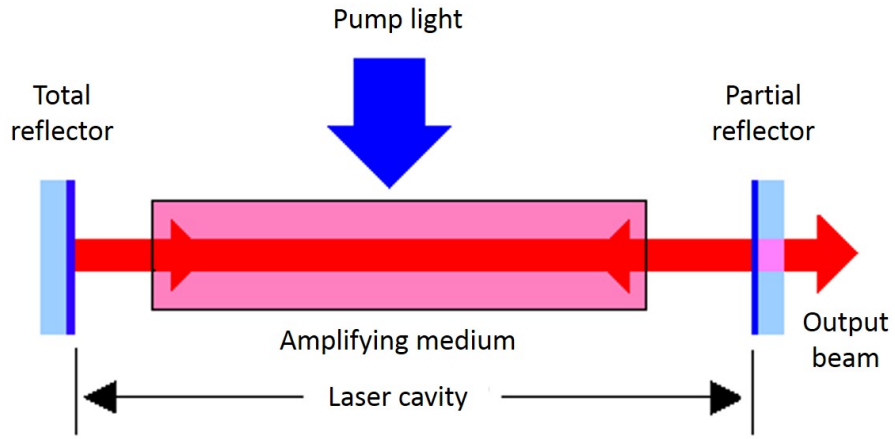

Figure 1.3: Schematic of a laser oscillator. Adapted from [3].

One of the mirrors shown in Figure 1.3 is partially reflective. The energy that is able to get transmitted through this mirror forms the output beam of a laser. Further discussion of laser oscillators and amplifiers can be found in [6].

1.2 Diode pumping of solid-state lasers

The three principal elements of a solid-state laser are as follows [11]:

- The host material with its macroscopic mechanical, thermal and optical properties, and its unique microscopic lattice properties.
- The activator/sensitizer ions with their distinctive charge states and free-ion electronic configurations. The host material is doped with these ions.
- The optical pump source with its particular geometry, spectral irradiance, and temporal characteristics. Examples include flashlamps, continuous-wave arc lamps, or diode lasers.

Solid state lasers with diode pump sources have certain advantages over solid state lasers with other pumping mechanisms, and have replaced flashlamp pumped lasers in many applications. The main advantages of laser diode pumping are as follows [11]:

- A high electrical-to-optical efficiency of the pump source (of the order of 50%) leads to a high overall power efficiency (wall-plug efficiency) of the laser. As a consequence, smaller power supplies are needed, and both the electricity consumption and the cooling demands are drastically reduced, compared with those for lamp-pumped lasers.
- The lifetime of laser diodes is long compared with that of discharge lamps: typically many thousands of hours, often even well above 10,000 hours with proper use.
- The narrow optical bandwidth of diode lasers makes it possible to pump directly certain transitions of laser-active ions without losing power in other

spectral regions. It thus also contributes to a high efficiency. Figure 1.4 [4] shows the absorption spectrum of Nd:YAG, as well as the emission spectrums of a flash pump and diode laser respectively. Nd:YAG is pumped at 808 nm, so that lasing at 1064 nm can be achieved (Figure 1.2). As seen in Figure 1.4, the narrow bandwidth of the diode laser enables pumping at the sharp absorption peak of 808 nm in Nd:YAG. In contrast, a flash lamp emits a broadband frequency spectrum, which includes frequencies that are not absorbed by Nd:YAG, as well as frequencies corresponding to Nd:YAG absorption peaks that do not contribute to lasing action at 1064 nm.

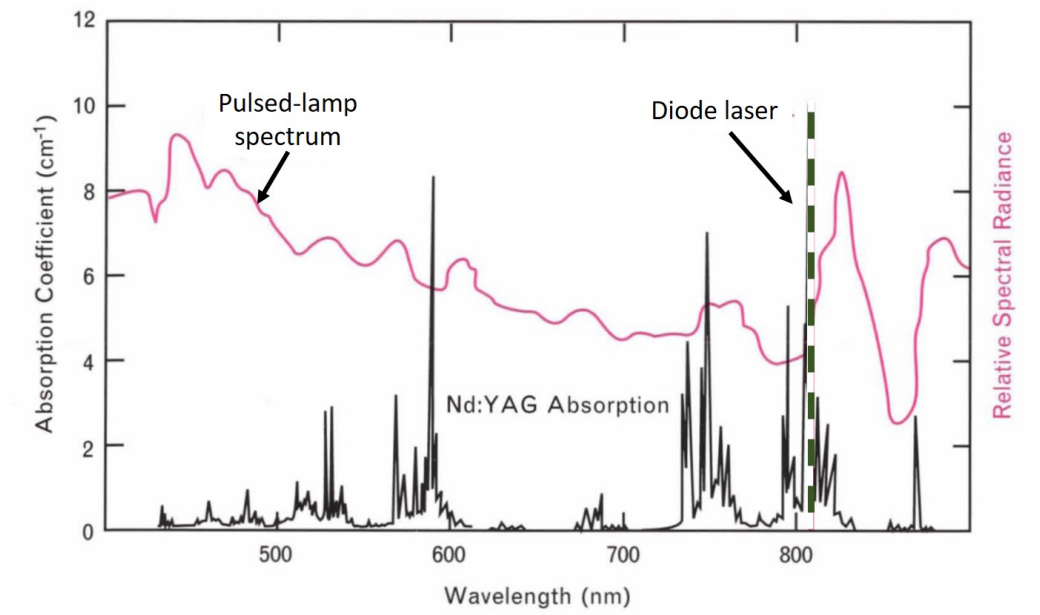

Figure 1.4: Absorption spectrum of Nd:YAG and the emission spectra of a diode laser and a pulsed flash lamp. The absorption spectrum is for Nd:YAG with 1% Nd doping. Adapted from [4].

1.3 Gain materials for diode pumped solid state lasers

The history of the development of lasers is described in detail in [6]. The conditions for laser action at optical frequencies were first described in 1958. The first demonstration of a solid state laser was achieved in 1960 using ruby (Cr^{3+}:Al_2O_3), a crystalline solid system. The next step in the development of solid-state lasers was the operation of trivalent uranium in CaF_2 and divalent samarium in CaF_2.

Laser action in neodymium-doped glass and the first continuously operating crystal laser using Nd^{3+}:$CaWO_4$ were reported in 1961. Since then laser action has been achieved by embedding trivalent rare earths (Nd^{3+}, Er^{3+}, Ho^{3+}, Ce^{3+}, Tm^{3+}, Pr^{3+}, Gd^{3+}, Eu^{3+}, Yb^{3+}), divalent rare earths (Sm^{2+}, Dy^{2+}, Tm^{2+}), transition metals (Cr^{3+}, Ni^{2+}, Co^{2+}, Ti^{3+}, V^{2+}), and numerous other dopants, in various host materials. Optically pumped laser action has been demonstrated in hundreds of ion-host crystal combinations covering a spectral range from the visible to the mid-infrared.

The exceptionally favorable characteristics of the trivalent neodymium ion for laser action were recognized at a relatively early stage in the search for solid-state laser materials. Thus, Nd^{3+} was known to exhibit a satisfactorily long fluorescence lifetime and narrow fluorescence linewidths in crystals with ordered structures, and to possess a terminal state for the laser transition sufficiently high above the ground state so that continuous-wave operation at room temperature was readily feasible. Therefore, this ion was incorporated as a dopant in a variety of host materials including, glass, $CaWO_4$, $CaMoO_4$, CaF_2, LaF_3, and so forth, in an effort to make use of its great potential. However, most of these early hosts displayed undesirable shortcomings, either from the standpoint of their intrinsic physical properties or

because of the way in which they interacted with the Nd^{3+} ions. Finally, yttrium aluminum garnet (YAG) was explored as a host for Nd^{3+}, and its superiority to other host materials was quickly demonstrated. As a result, Nd:YAG has become one of the most extensively deployed laser gain crystal material for diode pumped solid state lasers.

1.4 Nd:YVO_4 crystals

Neodymium-doped yttrium orthovanadate (Nd:YVO_4) is a crystalline material formed by doping yttrium orthovanadate with neodymium ions. As in numerous neodymium-doped laser crystals, the lasing action of Nd:YVO_4 is due to the neodymium ions, which can be excited by visible or infrared light, and undergo an electronic transition resulting in the emission of coherent infrared light, usually at a wavelength of 1064 nm. Figure 1.5 [5] shows shows the laser energy levels and laser transitions of Nd:YVO_4.

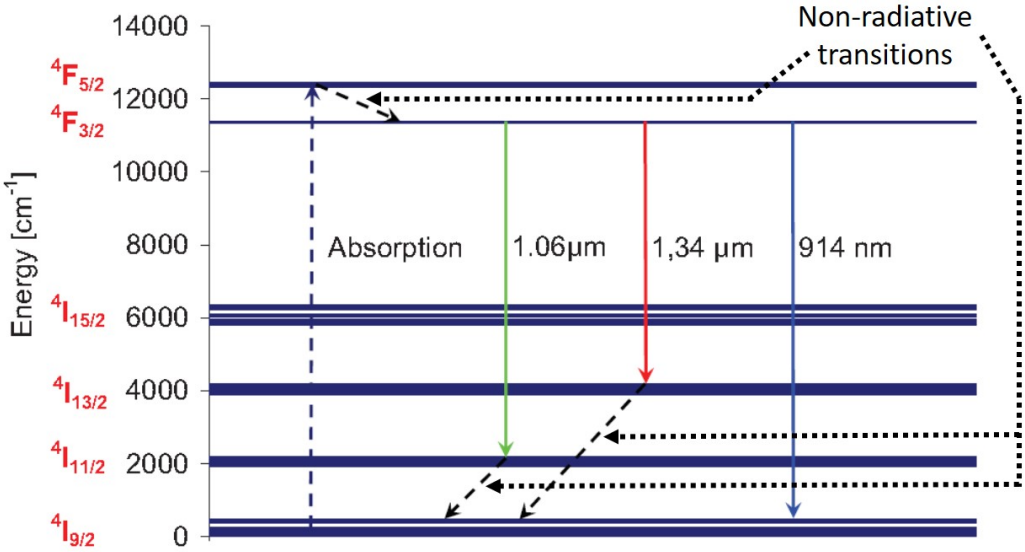

Figure 1.5: Laser energy levels and transitions of Nd:YVO_4. Adapted from [5].

1.5 Heat generation in laser crystals

In solid state lasers, a fraction of the absorbed pump energy get converted to heat, instead of contributing to lasing action inside the material. The fraction of the absorbed pump power that get converted to heat is known as the fractional heat load. Heat generation in crystals can be attributed to a number of non-radiative transition processes, which are defined as energy transitions that do not result in the emission of radiation (photons). A fundamental source of heat generation common to all laser crystals is the quantum defect (defined below). There are also processes involving higher energy levels which can add to the heat load of laser crystals. The two processes that predominate in Nd^{3+} doped materials are Auger upconversion (defined below) and excited state absorption (defined below). Details of the mechanisms of heat generation in laser crystals can be found in [5].

1.5.1 Quantum defects

The quantum defect is caused by the energy difference between the energy of the pump and lasing photons. The energy difference between the two is converted to heat and transferred to the crystal structure as phonons. The quantum defect is calculated by

$$q = 1 - \frac{\lambda_{pump}}{\lambda_{laser}} \tag{1.3}$$

For vanadate lasers that are pumped at $\sim$ 808 nm and operate on the 1 μm, 1.3 μm and 914 nm lines the quantum defect is $\sim$ 24%, 40% and 12% respectively.

The quantum defect is a significant contributor to the heat load for the 1 μm and 1.3 μm lines because of the large non-radiative transitions from the $^4I_{11/2}$ and $^4I_{13/2}$ lower laser levels to the $^4I_{9/2}$ ground state, respectively (Figure 1.5). In particular, out of all three laser lines shown in Figure 1.5, the lasing line at 1.3 μm

has the largest non-radiative transition between the lower laser level and the ground state, which leads to the highest heat generation in the crystal compared to the other lasing wavelengths (1 μm and 914 nm). The $^4F_{5/2}$ to $^4F_{3/2}$ transition generates extra heat for all three processes when 808 nm pump light is used. However, its contribution is small compared to the other two non-radiative transitions. The three level 914 nm transition therefore has the lowest heat generation from the quantum defect.

1.5.2 Auger upconversion

Auger upconversion is a process between two neighbouring active particles (atoms, molecules etc.) that are both in the upper laser level and is illustrated for a general four-level material in Figure 1.6 [5]. One of these active particles (atoms,

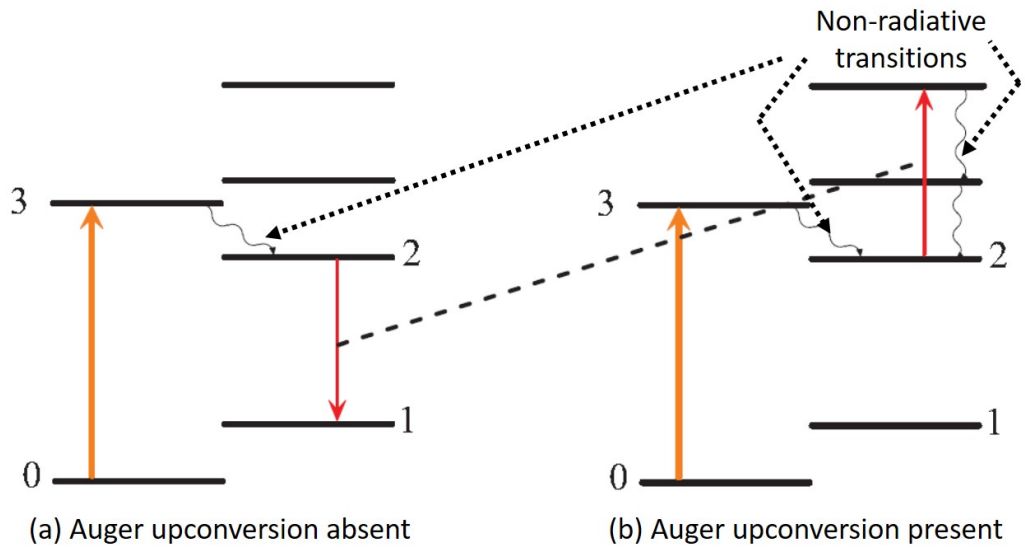

Figure 1.6: Auger upconversion in a four-level laser material. Adapted from [5].

molecules etc.) transfers its energy to the other which is excited into an even higher level. The particle (atom, molecule etc.) in the higher level then decays radiatively

and/or non-radiatively back to the upper laser level or lower energy levels. A particle (atom, molecule etc.) in the upper laser level is therefore lost and its energy converted into heat, infra-red and/or visible radiation. When compared to a transition process without Auger upconversion, it can be seen from Figure 1.6 that Auger upconversion leads to a greater probability of non-radiative transitions.

Upconversion is highly dependent on doping concentration. By increasing the doping concentration the average distance between active ions is effectively decreased, which increases the probability of energy transfer between them. Upconversion is also dependent on the number of active ions in the $^4F_{3/2}$ upper laser level and is therefore indirectly dependent on which transition stimulated emission takes place, since the inversion density is clamped at the lasing threshold. This implies that heat generated by upconversion can become severe under non-lasing conditions since the inversion is not clamped. In such cases an interruption of the lasing process in highly pumped crystals can lead to fracture of the laser crystal due to the extra generated heat.

From the characteristics discussed above, upconversion can be identified by higher fluorescence in the crystal during non-lasing conditions as well as a temperature decrease during lasing conditions.

1.5.3 Excited state absorption

In some materials there are higher energy levels (above level 3 in Figure 1.7) present which have an energy difference between them and the upper laser level (excited state) that is very close to either the pump or laser photon energies. Laser or pump photons are absorbed and the energy of some of the active particles (atoms, molecules etc.) in the upper laser level is raised to this even higher level. The particles (atoms, molecules etc.) in the even higher level then decay radiatively

and non-radiatively back to the upper or lower laser levels. A pump or laser photon is therefore lost and extra heat is generated within the crystal. This process is called excited state absorption (ESA) and is summarized for general four-level materials in Figure 1.7 [5]. From the characteristics discussed above it follows that excited state absorption manifests itself by increased temperature and fluorescence in the crystal during lasing conditions.

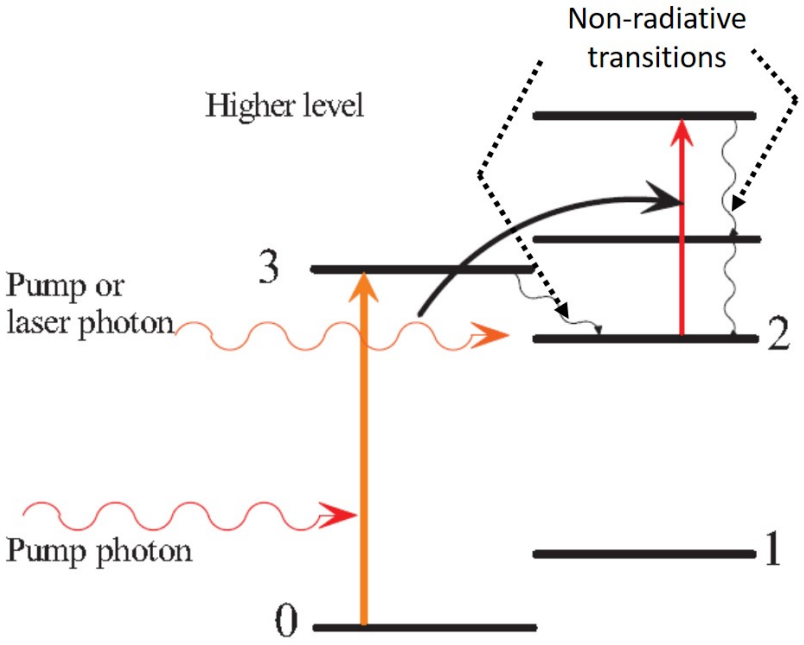

Figure 1.7: Excited state absorption of a pump or laser photon in a four-level laser material. Adapted from [5].

1.6 Thermal stress fracture in laser crystals

The heating of laser crystal due to optical pumping generates a temperature gradient inside the crystal, which in turn causes a thermal expansion gradient. The thermal expansion in turn results in the creation of stress inside the crystal, which can result in fracture once the stress limit is exceeded.

1.7 Advantages and limitations of $Nd:YVO_4$ as a laser gain medium

Nd:YAG is one of the most widely deployed laser gain crystals in diode pumped solid state lasers. A detailed discussion explaining the dominance of Nd:YAG as a laser gain medium can be found in [6]. However, one of the drawbacks of Nd:YAG is the narrow absorption bandwidth around the 808 nm wavelength. This requires the diode pump laser to have a stable peak wavelength as a function of time, which requires the temperature of the pump laser diode to be precisely controlled. This results in increased engineering, manufacturing, and maintenance costs for diode pumped solid state Nd:YAG lasers. Figure 1.8 [6] shows the output power of an $Nd:YVO_4$ and Nd:YAG laser, as functions of the pump diode laser wavelength and temperature. It can be seen that the output power of the $Nd:YVO_4$

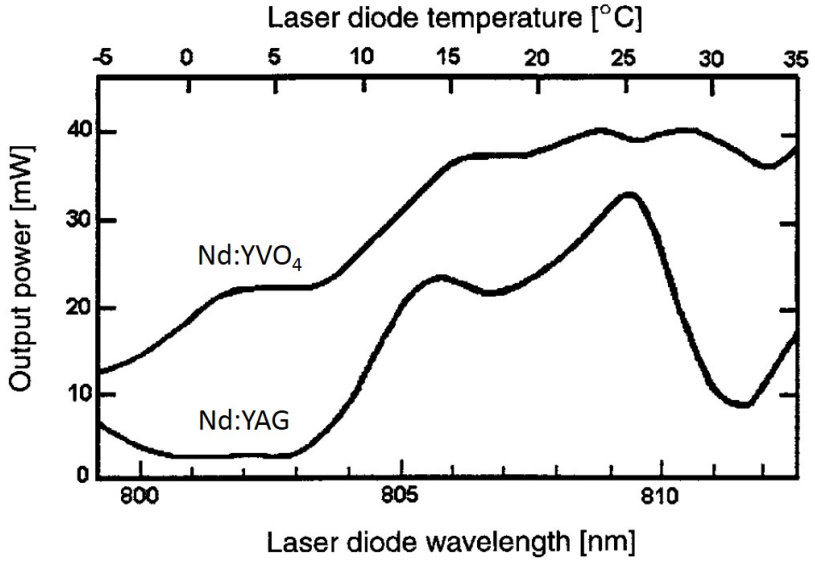

Figure 1.8: Output from an $Nd:YVO_4$ and Nd:YAG laser as a function of pump laser diode wavelength and temperature. Adapted from [6].

laser is smoother compared to that of the Nd:YAG laser, for pump diode wavelength ranging from 806 nm to 812 nm. Thus, $Nd:YVO_4$ has a lower dependency on the

pump diode wavelength compared to Nd:YAG. This reduces the demands of wavelength stability of the pump laser diode. Thus, Nd:YVO_4 has a greater tolerance for shifts in the pump diode laser wavelength, and hence can be used with a wider range of pump diodes. In addition, as the pump diode wavelength is a function of the diode temperature, Nd:YVO_4 requires less stringent temperature control of the diode temperature, which in turn reduces the requirements for precision temperature control equipment in the lasers. All these factors enable lower manufacturing and maintenance costs. In addition, Nd:YVO_4 has a higher laser cross section than Nd:YAG, which results in higher gain in Nd:YVO_4 in the case when both crystals are subject to the same optical pump power loading.

Although Nd:YVO_4 has numerous advantages over Nd:YAG, there are certain drawbacks as well. Principally, the thermal conductivity of Nd:YVO_4 is half of that of Nd:YAG [6]. As a result, it is harder to remove heat from Nd:YVO_4 crystals compared to Nd:YAG, for a given crystal cooling configuration. The low thermal conductivity also results in larger temperature gradient inside the crystal, when the crystal is subject to optical power loading. This makes Nd:YVO_4 vulnerable to thermal stress fracture. In fact, the thermal stress fracture limit for Nd:YVO_4 is three times lower than that of Nd:YAG [12]. Thus, thermal stress is a limiting factor in the deployment of Nd:YVO_4 as a gain medium in high power diode pumped solid state lasers. In addition, Nd:YVO_4 has a shorter excited state lifetime than Nd:YAG [6]. The excited state lifetime is a measure of the energy storage capability of the gain medium in pulsed operation. Large energy storage requires a long excited state lifetime, and thus the shorter excited state lifetime is an additional factor limiting the utility of Nd:YVO_4 in high power applications.

1.8 Scope of this work

In this thesis, thermal damage was experimentally investigated and simulated in a 3% Nd doped Nd:YVO_4 crystal. A 3% Nd doping is on the higher end for commercially available Nd:YVO_4 crystals. The higher the Nd doping, the smaller the absorption depth of the incident pump power. Thus, Nd:YVO_4 crystals with a high Nd doping are of interest for thin disk, high power laser applications. However, higher doping densities also result in increased heat generation inside the crystals, when it is subject to optical pumping. This in turn reduces the failure thresholds for laser induced melting and thermal stress damage in the crystals.

The 3% Nd doped crystal in the simulation and experiments in this thesis was not part of a laser oscillator, that is, no cavity mirrors were present in the simulation and experiment environments. The crystal was pumped with a high power diode laser, and the experimental melting threshold was compared with simulation results. In addition, the experimental thermal fracture threshold was also compared to the simulation results. The simulations for thermal damage in the 3% Nd doped crystal were then generalized to crystals with lower Nd doping and different geometries. Thus, the effects of Nd doping and crystal geometry were examined on the thermal heat and stress damage in Nd:YVO_4 crystals, in the absence of lasing.

CHAPTER 2

SIMULATIONS AND EXPERIMENTAL ANALYSIS OF EFFICIENCY OF OPTICS FOR COUPLING PUMP LASER INTO $Nd:YVO_4$ CRYSTALS

2.1 Introduction

In order to simulate the heating and thermal stress fracture induced by a laser in a crystal, it is essential to know the optical power that is getting coupled into the crystal. The diode pump laser bar (Jenoptik JOLD-72-CPFN-1L) used in the experiments had an emitter length of 10 mm, whereas the $Nd:YVO_4$ crystal that was used had a pumping face length of 3 mm. To account for this, an acylindrical lens (Thorlabs AYL-1815B) was used to focus the laser beam into the crystal. This optical coupling system was simulated in a Zemax environment, and the simulated power coupling efficiency was then compared to the experimental power coupling efficiency.

2.1.1 Zemax software

Zemax is a ray-tracing software that is used to design and analyze imaging, as well as illumination systems. Zemax can model numerous types of lenses, gratings, light sources, and detectors. In addition, Zemax can produce standard analysis diagrams such as ray-fan plots, spot diagrams, as well as optical power profile plots [13]. Zemax also has tolerancing capabilities to account for manufacturing errors, as well as environmental conditions, such as lens heating. Finally, Zemax also possesses optimization tools that can improve an initial optical design by adjusting different

parameters, to maximize the specified performance, such as the minimization of aberrations [14].

2.2 Zemax modeling

The entire optical system consisting of the laser diode bar, acylindrical lens, as well as the power meter was modeled in the non-sequential mode of Zemax.

2.2.1 Optical system layout

The flat end of the acylindrical lens was placed at a distance of 21 mm from the laser source diode in Zemax, with the curved surface facing the laser. The crystal surface was placed at a distance of 32.356 mm from the laser. These distances were obtained by running the optimization programs in Zemax to maximize the laser power that could be coupled into the crystal. Figure 2.1 [7] shows the top and side view of the laser source diode, acylindrical lens, and the crystal surface assembly in Zemax. The blue lines in the left subsection of Figure 2.1 represent the ray tracing done by Zemax.

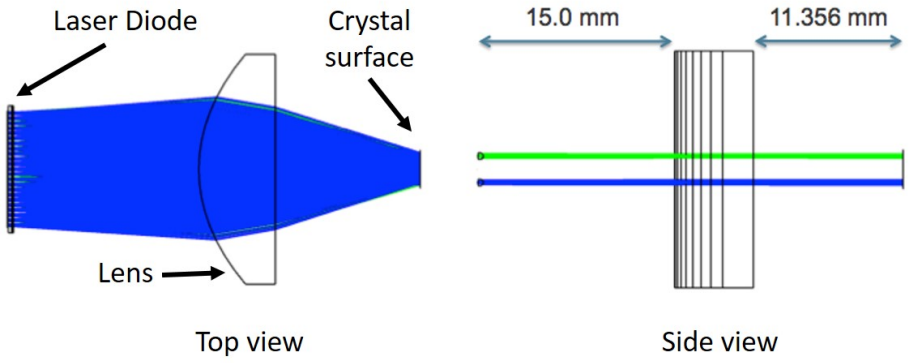

Figure 2.1: Top and side view of laser coupler system in Zemax. Adapted from [7].

2.2.2 Semiconductor diode pump laser

Table 2.1 shows the Zemax parameters for the laser diode bar used to pump the Nd:YVO_4 crystal.

Table 2.1: Zemax Parameters for the Pump Diode Laser Bar (Obtained from Manufacturer Datasheet)

Laser Parameter	**Value**
Wavelength	808 nm
Number of emitters	47
Emitter pitch	0.212 mm
Fast axis divergence (y-divergence)	0.5°
Slow axis divergence (x-divergence)	9°
Analysis rays	200000

The analysis rays are used to obtain incident optical power profile on the surface of the crystal. Hence, it is essential to use a large number of rays ($\geq$100000) to obtain convergence of results.

2.2.3 Acylindrical lens

Given the emitter length (10 mm) and divergence of the pump diode laser bar, as well as the dimensions of the pump face of the crystal (3×3 mm), an acylindrical lens with a back focal length (BFL) of 11.6 mm was used to maximize the amount of laser power that could be coupled into the crystal. An acylindrical lens is a type of lens with a translational symmetry whose surface profile deviates from that of a perfect cylinder, given by equation 2.1 [15]

$$z = \frac{r^2}{R(1+\sqrt{1-(1+k)\frac{r^2}{R^2}})} + A_4 r^4 + A_6 r^6 + A_8 r^8 + A_{10} r^{10} \tag{2.1}$$

where z is the saggita of the surface parallel to the optical axis, r is the radial distance, R is the radius of curvature, and k is the conic constant. The coefficients

A_4, A_6, A_8 and A_{10} describe the deviation from the axially symmetric quadratic surface specified by R and k. Figure 2.2 [8] shows an acylidrical lens.

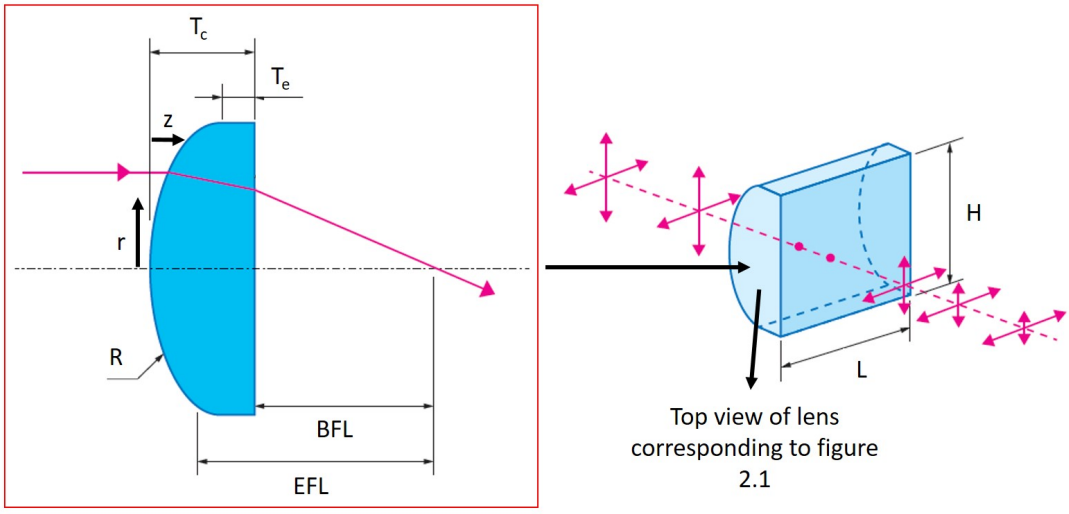

Figure 2.2: Schematic of an acylindrical lens. Adapted from [8].

Table 2.2: Zemax Parameters for the Acylindrical Lens (Obtained from Manufacturer Datasheet).

Lens Parameter	**Value**
Material	S-LAH64 Glass
Radial height (L)	9 mm
X half-width (H)	9 mm
Thickness (T_c)	6 mm
Radius (R)	11.653 mm
Z tilt	90°
Coating	Anti-reflective
Conic	-0.541
A_4	-7.5260568 $\times$ 10^{-6}
A_6	-7.2065825 $\times$ 10^{-8}
A_8	-2.7040888 $\times$ 10^{-10}
A_{10}	-5.5002321 $\times$ 10^{-13}

An aspheric lens exploits the deviations from the spherical surface to reduce

or eliminate spherical aberration, and also reduce other aberrations, such as astigmatism, compared to a simple lens. A single aspheric lens can often replace a much more complex multi-simple lens system, which can reduce the size, weight and cost of these optical systems, while also improving performance [16]. Table 2.2 shows the Zemax parameters for the acylindrical lens used in this thesis. Variables in brackets correspond to Figure 2.2.

2.2.4 Crystal surface

The detector surface tool in Zemax was used to model the side of the Nd:YVO_4 crystal that was facing the pump laser diode bar. The surface square was modeled as a perfect absorber, as the parameter of interest was the power that was incident on the face of the crystal, not the power absorbed by the crystal. Table 2.3 shows the Zemax parameters for the detector surface.

Table 2.3: Zemax Parameters for the Crystal Surface

Crystal surface Parameter	**Value**
Material	ABSORB
X half-width	1.5 mm
Y half-width	1.5 mm
X Pixels	100
Y Pixels	100

2.3 Experimental setup

2.3.1 Optical bench layout

The basic layout of the experimental setup is similar to that shown in Figure 2.1. The only difference is that instead of the crystal, a aluminium plate with an aperture of 3×3 mm was used. A power meter (Thorlabs S302C thermal sensor)

was placed immediately after the aperture, to minimize losses due to the beam divergence, and thus maximize the power incident on the power meter detector surface. The thermal sensor was then connected to a power meter (Thorlabs PM100A power meter). Figure 2.3 shows the schematic of the experimental setup.

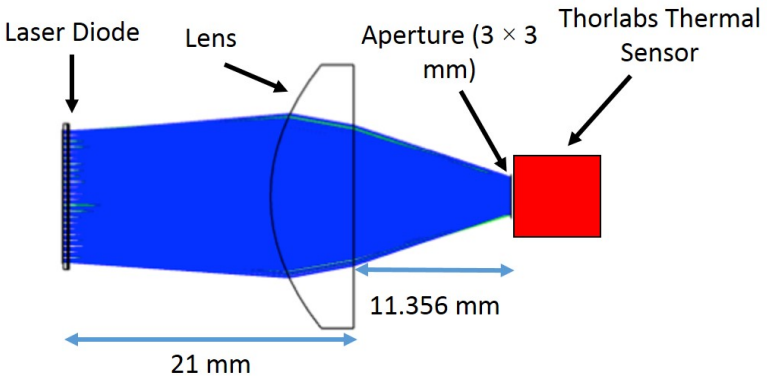

Figure 2.3: Top view schematic of the direct power measurement experimental setup (only for up to 2 W of optical power incident on the sensor)

However, the setup shown in Figure 2.3 can only be used as long as the power incident on the thermal sensor is less than 2 W, in order to prevent optical damage to the sensor. However, to study thermal damage in the crystal, it was essential to reach much higher laser output optical powers ($\geq$70 W). In order to prevent optical damage to the thermal sensor, a microscope glass slide was mounted at an angle of 45° after the aperture plate, as shown in Figure 2.4. The slide acted like a beam splitter, with 1.25% of the incident power being reflected at an angle. This reflected beam was then guided onto the thermal sensor. Thus, the reflected power measurement was then used to estimate the total optical power getting coupled through the aperture, enabling the setup shown in Figure 2.4 to be used for optical powers greater than the 2 W detection limit of the thermal sensor.

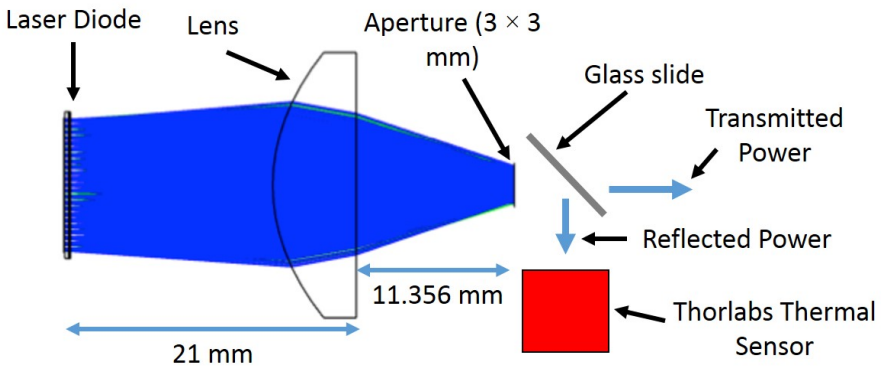

Figure 2.4: Top view schematic of the indirect power measurement experimental setup

2.3.2 Laser thermal management

It was necessary to cool the laser source diode in order to prevent thermal failure of the semiconductor bars, according to the manufacturer datasheet. For the experiments, a copper block with refrigeration coolant channels was machined. Deionized water was pumped through the block, with the water being cooled by a thermoelectric chiller (Thermotek T255P). The laser bar was mounted on the copper block, as shown in Figure 2.5.

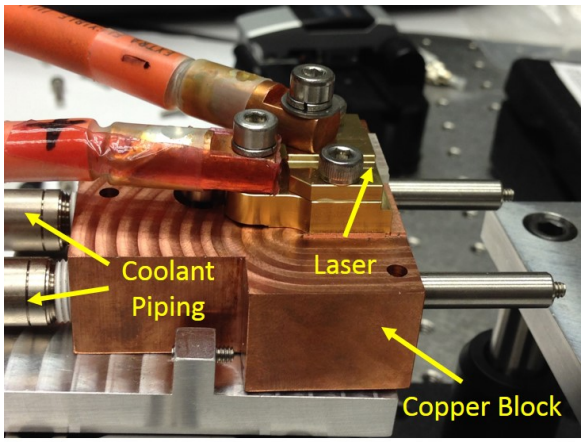

Figure 2.5: Cooling setup of the laser diode bar

2.4 Comparison of simulations and experimental results

The manufacturer data for the laser drive current vs. the output optical power was used as the starting point. According to the datasheet, the threshold current of the laser was 19.3 Amps. Some irregularities were observed in the beam shape and divergence of the laser up to a drive current of 25 Amps, which might have been caused by operation near the laser threshold current. Since the laser beam shape and divergence are crucial parameters for Zemax, the laser output optical power corresponding to 30 Amps of drive current was chosen as the starting point of the simulations, as the beam characteristics were consistent by the optical power corresponding to that drive current. Thus, the Zemax simulation design shown in Figure 2.1, in addition to the indirect power measurement experimental setup shown in Figure 2.4, were used to estimate the power getting coupled into a 3×3 mm crystal face, for laser drive currents ranging from 30 to 80 Amps. Figure 2.6 shows the results for the simulations and the experiments.

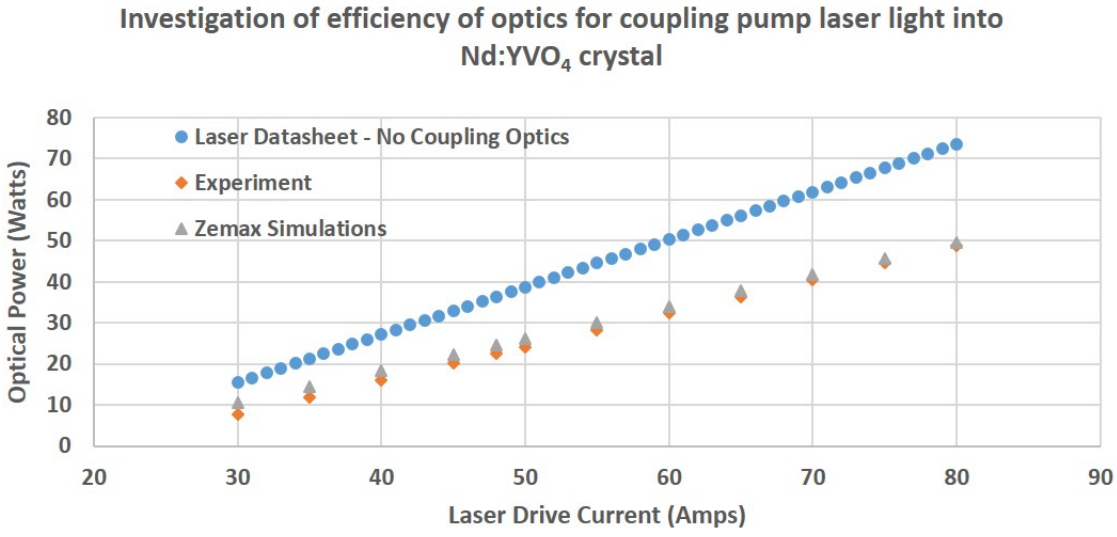

Figure 2.6: Simulations vs. experimental results for laser coupler efficiency

Also shown in Figure 2.6 is the datasheet laser output optical power, as a function of the drive current. It can be seen that the acylindrical lens cannot couple all of the optical power of the laser into the 3×3 aperture, as seen by the difference between the laser datasheet powers and the simulation as well as experimental results. It can be seen from Figure 2.7 that when the laser output optical power was

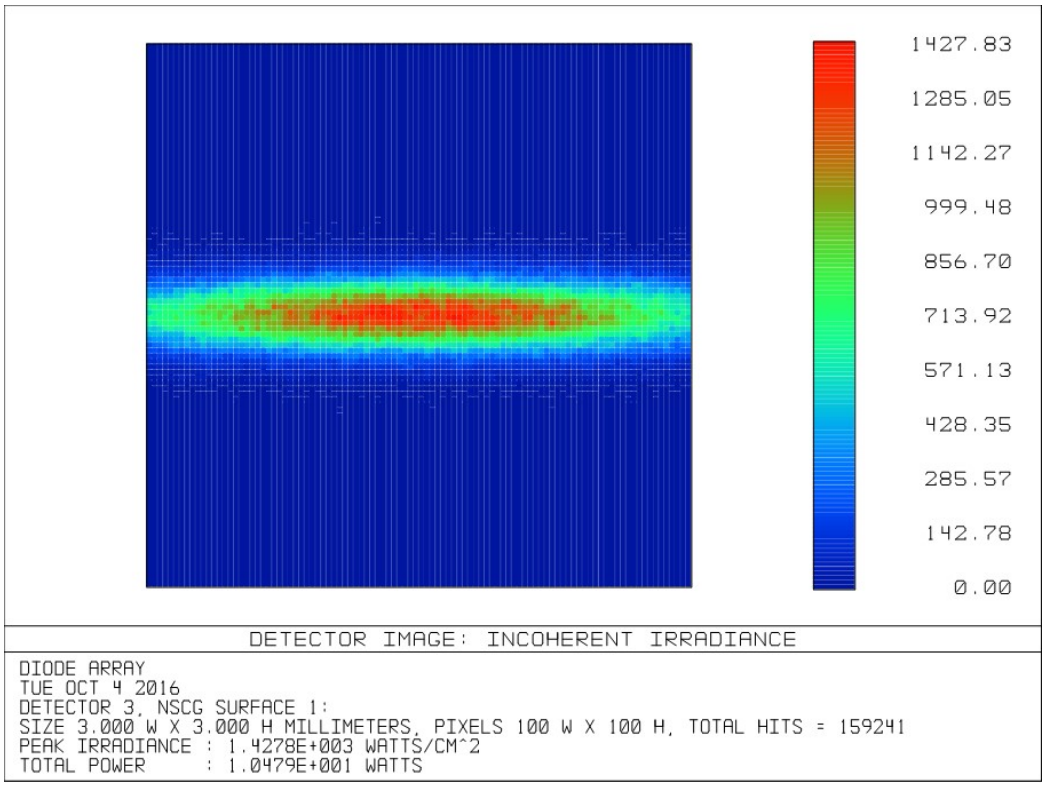

Figure 2.7: Zemax simulation of the profile of the pump laser optical power incident of the 3×3 mm face of the crystal.

set to 15.5 W, about 10.45 W was coupled into the crystal, according to the Zemax simulation for the optical system shown in Figure 2.1. It is evident from Figure 2.7 that the ends of the laser spot have been chopped off, and cannot be coupled into the crystal, thus resulting in a coupling power loss. The coupling efficiency could be improved with the use of a more advanced optical systems, consisting of multiple

lenses, to focus the laser beam more tightly on the crystal. However, the main intention was to have a region of relatively uniform pumping on the crystal, which the above system achieved.

Thus, the Zemax simulations were compared to the experimental results, and both were found to be in agreement. With the experimental verification of the simulations of the optical power getting coupled into the crystal, further simulations were carried out to study the laser induced heating as well as the laser induced thermal stress fracture in Nd:YVO_4 crystals, both in the absence of stimulated emission.

CHAPTER 3

SIMULATION OF LASER INDUCED HEATING IN $Nd:YVO_4$ CRYSTALS

3.1 Introduction

An $Nd:YVO_4$ crystal with an Nd doping of 3% was simulated in a Zemax environment. The Zemax optical power coupling efficiency simulations from chapter 2 were then used in conjunction with LASCAD, a finite element analysis software, to obtain the maximum temperatures reached inside the crystal as a function of the laser drive current. The simulations were then compared to experimental results of the laser induced heating of the crystal. Lastly, the simulations were generalized to different crystal geometries and Nd doping concentrations.

3.2 Modeling of $Nd:YVO_4$ in Zemax

Zemax has an extensive catalog of industry standard glasses that can be used when designing and simulating optical elements. In addition, Zemax also enables to the user to modify or define new optical glasses and materials. The $Nd:YVO_4$ crystal was defined as a custom material in Zemax by specifying the refractive index and transmission as a function of the wavelength. A variation of the Sellmeier formula used to model the dispersion of the crystal is given by equation 3.1 [14].

$$n^2 = A + \frac{B}{\lambda^2 - C} - D\lambda^2 \tag{3.1}$$

where n is the refractive index, and λ is the wavelength (μm). Table 3.1 states the coefficients A,B,C and D that were used to model the dispersion in Zemax [14].

Table 3.1: Glass Dispersion Coefficients

Glass dispersion coefficient	**Value**
A	3.77879
B	7.479×10^{-2} μm^2
C	4.5731×10^{-2} μm^2
D	9.701×10^{-3} μm^{-2}

The transmission of the crystal for a wavelength of 808 nm was calculated from the absorption coefficient α

$$\alpha = n_{Nd} \times \sigma_{abs} \times (1 - f_{lower}) \tag{3.2}$$

where n_{Nd} is the neodymium dopant density, σ_{abs} is the neodymium absorption cross section, and f_{lower} is fraction of the population in the lower state. The neodymium dopant density (n_{Nd}) is

$$n_{Nd} = \frac{n_{Yt} \times Nd\%}{100} \tag{3.3}$$

where n_{Yt} is yttrium site density, and $Nd\%$ is the neodymium doping density. The fraction of the population in the lower state (f_{lower}) is

$$f_{lower} = exp\Big(\frac{-E_{lower}}{kT}\Big) \tag{3.4}$$

where E_{lower} is the energy of the lower lasing level of neodymium, and T is the temperature. Table 3.2 shows the values of the parameters in equations 3.2, 3.3 and 3.4 that were used to calculate the absorption coefficient of Nd:YVO_4 with a Nd doping of 3%. Thus, the absorption coefficient was calculated for a temperature range from 288 K to 2098 K. A temperature of 288 K corresponds to lowest coolant temperature set point in the experimental setup for cooling the crystal, and 2098 K corresponds to the melting point of Nd:YVO_4 [17].

Table 3.2: Parameters for Calculation of Absorption Coefficient of Nd:YVO_4 with 3% Nd doping

Parameter	Value
Yttrium site density (n_{Yt})	1.2462 $\times$ 10^{22} cm^{-3}
Neodymium doping($Nd\%$)	3%
Energy of lower lasing level of Neodymium(E_{lower})	4.19 $\times$ 10^{-20} Joules
Temperature (T)	288 - 2098 K

The absorption length, which is defined as the distance into the material where the beam power has dropped to $\frac{1}{e}$ of the incident power, was calculated using

$$l_{absorption} = \frac{1}{\alpha} \tag{3.5}$$

where α is the absorption coefficient obtained from equation 3.2. Figure 3.1 shows the absorption length for an Nd:YVO_4 crystal with a 3% Nd doping as a function of temperature.

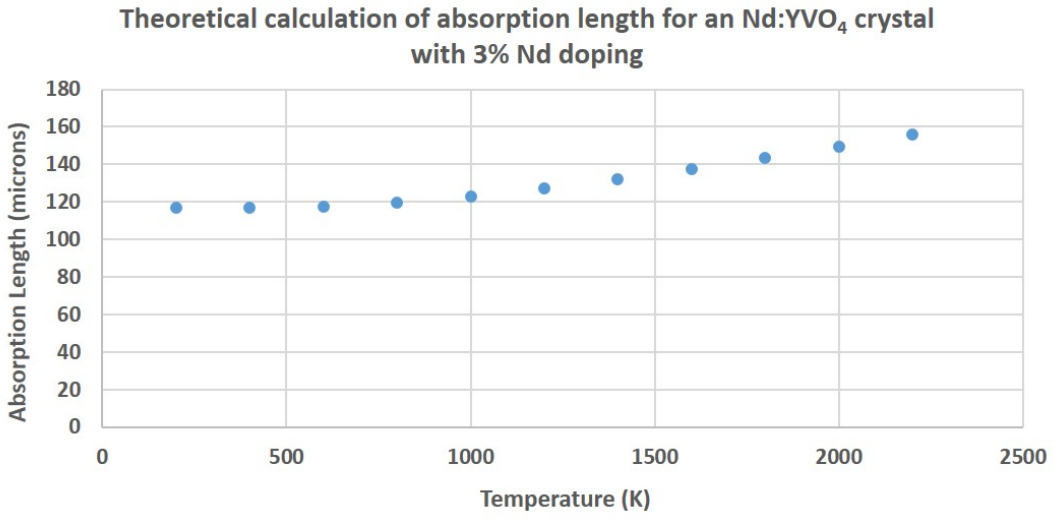

Figure 3.1: Absorption length vs. temperature for an Nd:YVO_4 crystal with a Nd doping of 3%

It can be seen from Figure 3.1 that the absorption length increases by

approximately 1.5% from about 300 K to 2100 K. This increase in absorption length (30 μm) is negligible compared to the length of the crystal (2000 μm). As the temperature approaches the melting point of Nd:YVO_4 ($\approx$ 2098 K), the absorption length is approximately 150 μm. It was assumed that at twice the absorption length, almost all the optical power incident on the crystal would have been absorbed by the crystal. This assumption is consistent over the entire temperature range of interest (room temperature to melting point of Nd:YVO_4), as the absorption length decreases as the temperature decreases. Thus, this theoretically calculated absorption information was then modeled into the Zemax environment, as seen in table 3.3.

Table 3.3: Zemax Absorption Parameters for Nd:YVO_4 with 3% Nd doping

Wavelength	**Transmittance**	**2 $\times$ Absorption length**
808 nm	0%	300 μm

3.2.1 Optical system layout

The optical system layout in Zemax for laser optical coupler and crystal assembly is shown in Figure 3.2. Note that this layout is similar to that in Figure 2.1, except that the actual crystal was simulated in Zemax, instead of an absorbing surface. The crystal in the Zemax environment had a length of 2 mm, and a width and height of 3 mm. The Zemax simulations of the incident optical power profile on the absorbing surface (from chapter 2) were used in conjunction with the custom Nd:YVO_4 material that was defined in Zemax, to obtain the Zemax simulations for the absorbed optical flux density profile inside the crystal.

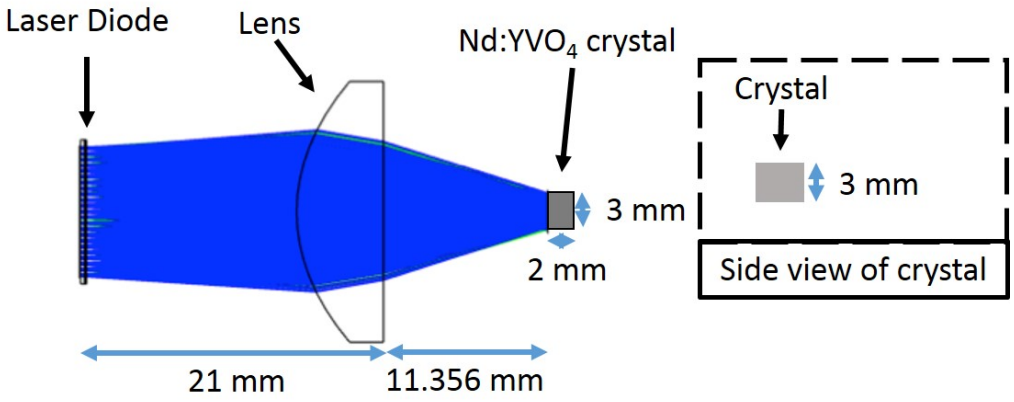

Figure 3.2: Top view of laser coupler and crystal assembly in Zemax

3.3 Laser induced heating of $Nd:YVO_4$ with and without stimulated emission

In an $Nd:YVO_4$ based diode pumped solid state laser, a fraction of the absorbed pump power is converted to heat, rather than contributing to the stimulated emission, that is, the lasing process. Experimental studies have shown that for an $Nd:YVO_4$ crystal with a Nd doping of 3%, that was pumped with a wavelength of 808 nm, about 45% ($\pm$ 3%) of the absorbed pump power is converted to heat, when the crystal was part of a laser oscillator, with a laser emission wavelength of 1064 nm [18, 19].

On the other hand, it has been found that for an $Nd:YVO_4$ crystal, subject to the same doping and pumping conditions, the percentage of absorbed optical pump power converted to heat is approximately doubled when the crystal was not part of a laser oscillator, compared to when the crystal was part of a laser oscillator [20]. This means that an $Nd:YVO_4$ crystal subject to laser pumping will heat up to a greater degree if the crystal is not part of a laser oscillator, compared to if the laser pumped crystal was part of a laser oscillator.

3.4 Finite element analysis with Zemax and LASCAD

The Zemax simulations for the absorbed flux density were obtained as a function of the laser optical output power, and the results were exported to LASCAD, a finite element analysis software which is optimized for laser cavity design and analysis. The absorbed flux density supplied by Zemax was converted into a temperature profile by LASCAD. Thus, the maximum temperature reached inside the crystal was obtained as a function of the absorbed pump power (The absorbed pump power is the integral of the absorbed flux density).

3.4.1 Theoretical background

Finite element analysis (FEA) is a numerical method for predicting how an object (in the case of this thesis, a laser crystal) reacts to various loading fields, such as heat, fluid flow, pressure, electromagnetic radiation, and other physical effects [21]. FEA works by first breaking down a real object into a large number of smaller finite elements, and then reconnecting the elements at nodes, as seen by an example shown in Figure 3.3 [9].

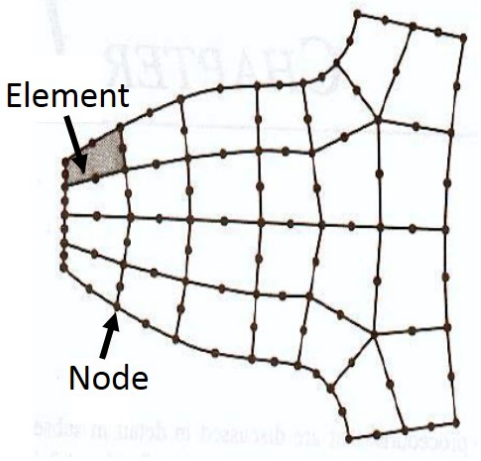

Figure 3.3: FEA Mesh. Adapted from [9].

Then, the effects of the loading fields on each element are predicted, and a set of simultaneous equations are obtained, as given by equation 3.6 [9].

$$[K]\{u\} = \{F\} \tag{3.6}$$

where K is the property of the material, u is the behaviour, and F is the loading force. Table 3.4 shows some common examples of the parameters in equation 3.6.

Table 3.4: Common Examples of Parameters in FEA Simultaneous Equations

Property $[K]$	**Behaviour $\{u\}$**	**Action $\{F\}$**
Elastic stiffness	Displacement	Force
Thermal conductivity	Temperature	Heat source
Fluid viscosity	Velocity	Body force
Dielectric permittivity	Electric potential	Charge

Equation 3.6 is then solved for the behaviour parameter u, as shown by equation 3.7 [9].

$$\{u\} = [K]^{-1}\{F\} \tag{3.7}$$

Thus, the values of the behaviour u of the finite element block are obtained at the nodes, given the property value K and the action value F supplied by the user. The finite element blocks are then connected together to obtain the values of the behaviour u over the entire system that is being studied. It should be noted that the values of the behaviour u obtained by FEA are not continuous, that is, the values are obtained at the nodes shown in Figure 3.3. As a result, decreasing the size of the finite element block increases the intervals of the nodes, which leads to values of the behavior u being obtained at shorter intervals. This in turn increases the accuracy of the FEA results. For a stable FEA simulation, the values of the behaviour u should converge as the element size approaches zero. For example, in

regards to this thesis, the maximum temperature inside the crystal should converge as the mesh size approaches zero.

Thus, FEA is especially useful for problems with complicated geometries, loading fields, and material properties, where analytical solutions are difficult to obtain. In addition, FEA also reduces the simplifications and idealizations used in analytic methods, thus increasing the accuracy of the results, enabling design optimization and tighter tolerances [9].

3.4.2 LASCAD parameters

Table 3.5 shows the parameters of the Nd:YVO_4 crystal with a Nd doping of 3%, that was modeled in LASCAD.

Table 3.5: LASCAD Parameters for Nd:YVO_4 with 3% Nd doping

LASCAD Parameter	**Value**
Crystal length (along z axis)	2 mm
Crystal width (along x axis)	3 mm
Crystal height (along y axis)	3 mm
Thermal conductivity	5.1×10^{-3} W/mm K
Coefficient of thermal expansion (along x and y axes)	4.4×10^{-6} 1/K
Coefficient of thermal expansion (along z axis)	1.137×10^{-5} 1/K
Elastic modulus	86000 N/mm^2
Poisson's ratio	0.3
Refractive index	1.958
Temperature dependence of refractive index	8.3×10^{-6} 1/K
Heat efficiency factor	0.98
Crystal top surface temperature	288 - 298 K
Crystal bottom surface temperature	288 - 298 K

The heat efficiency factor listed in table 3.5 is the fraction of the absorbed

laser pump power that is converted to heat in an Nd:YVO_4 crystal with 3% Nd doping, when the crystal is not part of a laser cavity, that is, in the absence of stimulated emission. Thus, the parameters in table 3.5 were used by LASCAD to convert the Zemax simulations of the absorbed optical flux density to a temperature data.

3.5 Experimental setup

The experimental setup used to investigate the laser induced heating of an Nd:YVO_4 crystal, with a Nd doping of 3%, is shown in Figure 3.4.

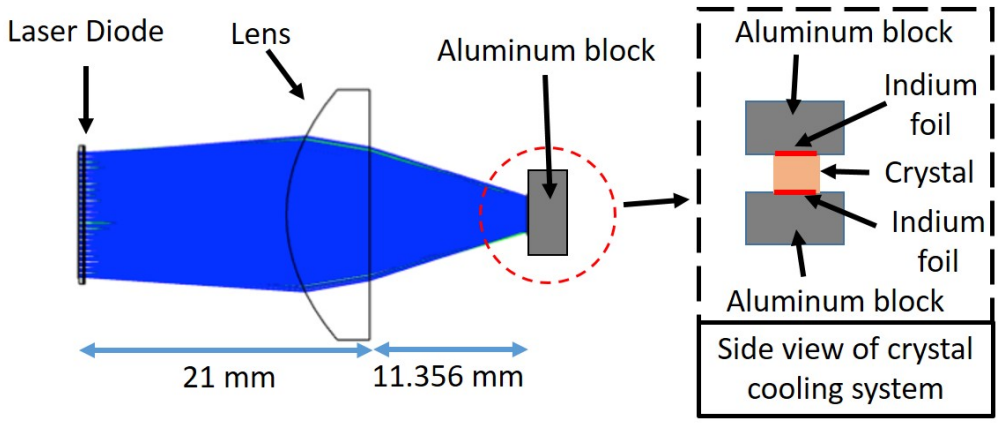

Figure 3.4: Top view schematic of experimental setup for investigating laser induced heating of an Nd:YVO_4 crystal. Also shown is the side view schematic of the laser crystal cooling setup

The crystal (Altechna 3-ND30YVO-06) was sandwiched between aluminium blocks coated with indium foil (the indium foil provides good thermal conductivity at the surfaces), as shown in the side view schematic in Figure 3.4. In addition, the laser was mounted on a copper block, as shown in Figure 2.5. The copper and aluminium blocks had refrigeration channels, through which chilled deionized water was pumped. This was done to prevent thermal failure of the laser, as well as study

the effect of cooling on the laser induced heating of the crystal.

3.6 Comparison of simulations and experimental results

A laser drive current of 30 Amps was used as a starting point of the simulations and experiment, due to issues with the beam shape and divergence below a drive current of 25 Amps (details in chapter 2). The maximum temperature reached inside the crystal was obtained from the Zemax and LASCAD simulations, for a given absorbed flux density profile. The absorbed flux density profile corresponds to the laser optical power that is coupled into the crystal, which in turn corresponds to the laser drive current. Thus, the simulations for the maximum

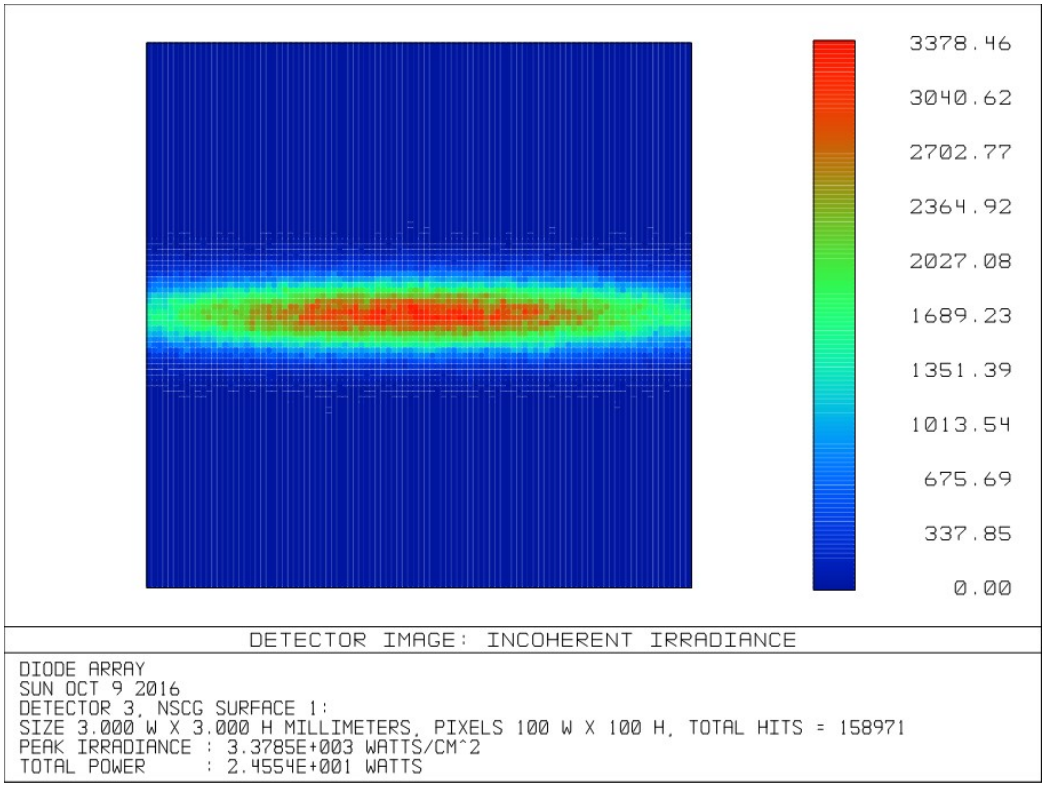

Figure 3.5: Zemax generated optical power profile of laser light incident on crystal, at a laser drive current of 48 Amps.

temperature inside the crystal were obtained as a function of the laser drive current, ranging from 30 to 80 Amps, with the 80 Amps upper limit being determined by the maximum drive current stated in the laser manufacturer datasheet.

During the Zemax and LASCAD Simulations, it was found that at a laser optical output power corresponding to 48 Amps, the maximum temperature reached inside the crystal was about 2102 K, which is 4 K (0.19%) greater than the melting point of Nd:YVO_4 (2098 K). Figure 3.5 shows the optical power profile of the laser light coupled into the crystal, for a laser drive current of 48 Amps, which corresponds to a laser optical output power of 36.4 W. It can be seen from Figure 3.5 that about 24.6 W of optical power was coupled into the crystal. Figure 3.6 shows the LASCAD generated temperature profile of the crystal, using the Zemax absorbed flux density data for a laser drive current of 48 Amps. The temperature of

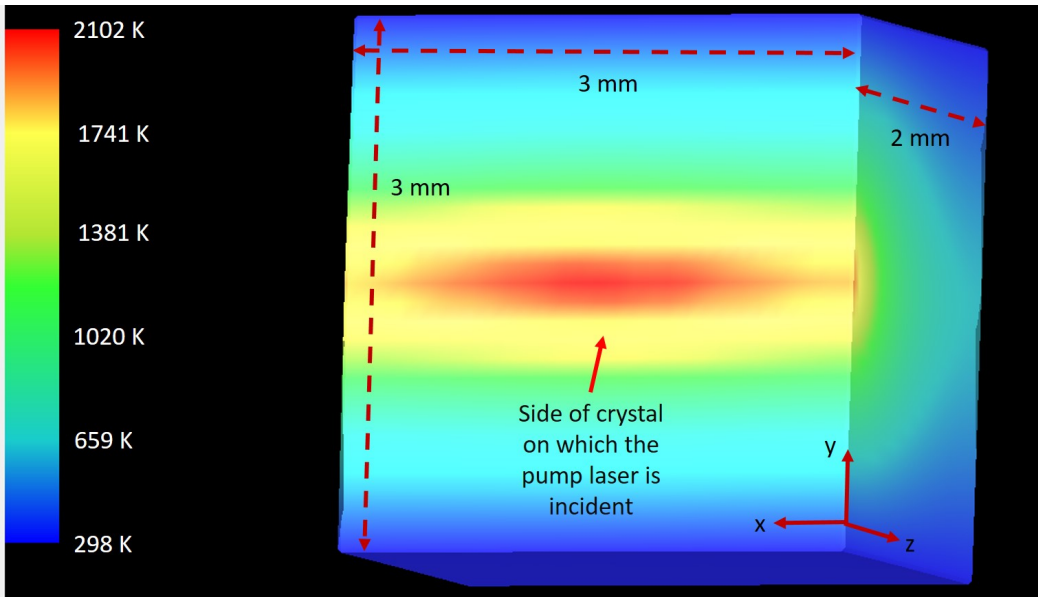

Figure 3.6: LASCAD generated temperature profile of crystal, at a laser drive current of 48 Amps.

the top and bottom surface of the crystal in the LASCAD simulation shown in

Figure 3.6 was set to 298 K, which was the temperature of the coolant that pumped through the crystal cooling system shown in Figure 3.4.

When the laser drive current was ramped up in the experimental setup shown in Figure 3.4, it was observed that the crystal started to melt at a laser drive current of 48 Amps, which corresponds to an optical power of 24.6 W being coupled into the crystal, as seen by Figure 3.5. Thus, the experimental results are in agreement with the Zemax and LASCAD simulations. Figure 3.7 shows the laser induced heating damage to the crystal used in the experiments.

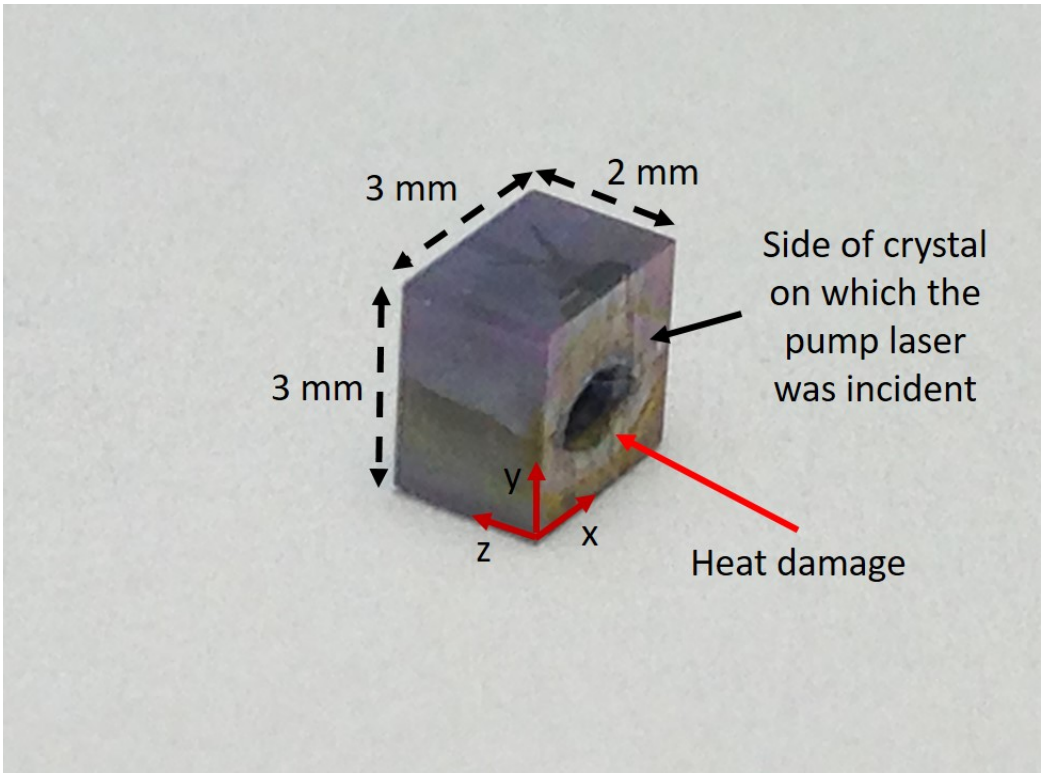

Figure 3.7: Laser induced heat damage in an Nd:YVO_4 crystal.

It can be seen from Figure 3.7 that the damage was concentrated at the center of the face of the crystal on which the pump laser light was incident. This corresponds to region of the highest optical power densities, as seen by the red

regions in the optical power profile in Figure 3.5.

Figure 3.8 summarizes the results for the simulations and experiment for the investigation the laser induced heating of the Nd:YVO_4 crystal with a Nd doping of 3%.

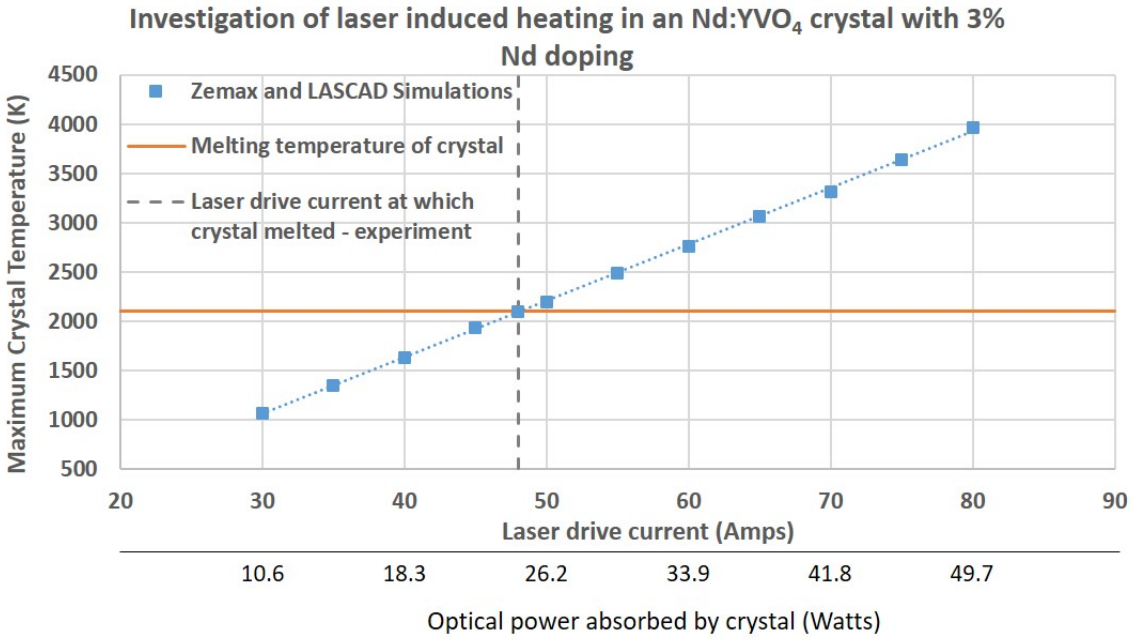

Figure 3.8: Comparison of simulations vs. experimental result for investigation of laser induced heating in an Nd:YVO_4 crystal.

3.6.1 Generalization of simulations - crystal geometry

The geometry of the laser crystal influences the efficiency of the crystal cooling mechanism. For instance, the efficiency of a cooling system increases if the heat sinks are placed closer to the heating load, which in this case, is the section of the crystal where the optical pump power is absorbed. Thus, the maximum temperature reached inside a laser crystal is a function of the crystal geometry, for a given absorbed optical power and crystal cooling system. Since the crystal used in

the experiments in this thesis had a thickness of 3 mm (crystal height in table 3.5), simulations were carried out to study the effect of reducing the thickness on the laser induced heating, for the same crystal cooling system shown in Figure 3.4. A thickness of 1 mm was chosen, which ensured that there were no additional optical power coupling losses, compared to the crystal with a thickness of 3 mm. Figure 3.9 shows the LASCAD generated temperature profile of a 1 mm thick Nd:YVO_4 crystal with a Nd doping of 3%, subject to the same optical power loading (24.6 W) and crystal cooling, at which the crystal with a thickness of 3 mm started to show heat damage in the experiment in Figure 3.4. It can be seen that the maximum

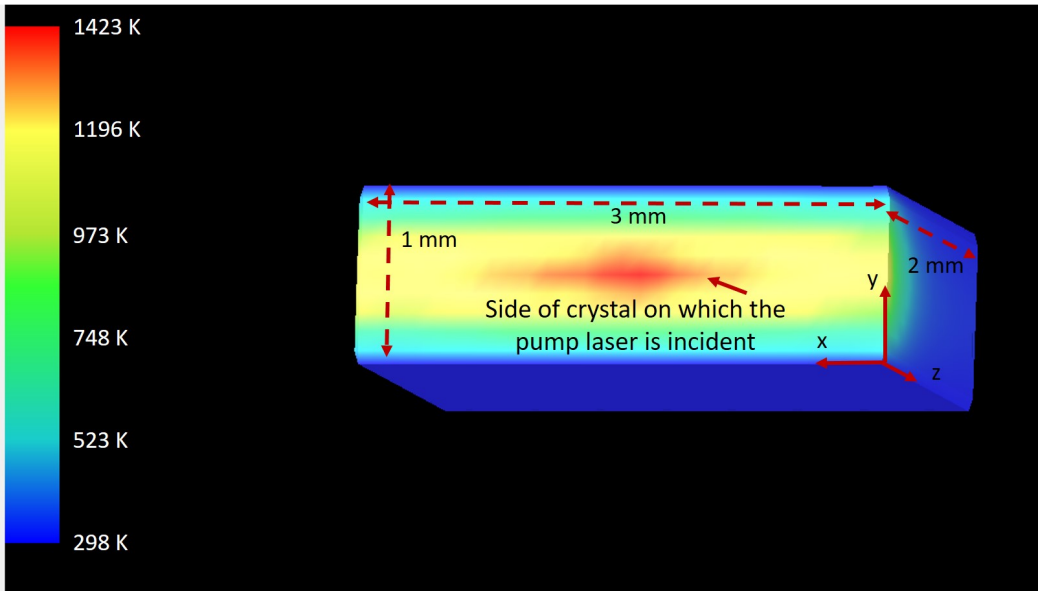

Figure 3.9: LASCAD generated temperature profile of 1 mm thick crystal, subject to the same optical power loading for the crystal with a thickness of 3 mm modeled in figure 3.6.

temperature reached inside the 1 mm thick crystal is well below the melting point of Nd:YVO_4 (2098 K), even though the crystal with a thickness of 3 mm suffered heat damage when it was subject to the same optical power loading and crystal cooling conditions.

Figure 3.10 summarizes the simulation results for the Nd:YVO_4 crystals with a thickness of 1 and 3 mm, subject to the same optical power loading by the pump laser diode. In addition, both crystals in the simulations were cooled from top and bottom surfaces, with the temperatures of these surfaces being set to 298 K. It can

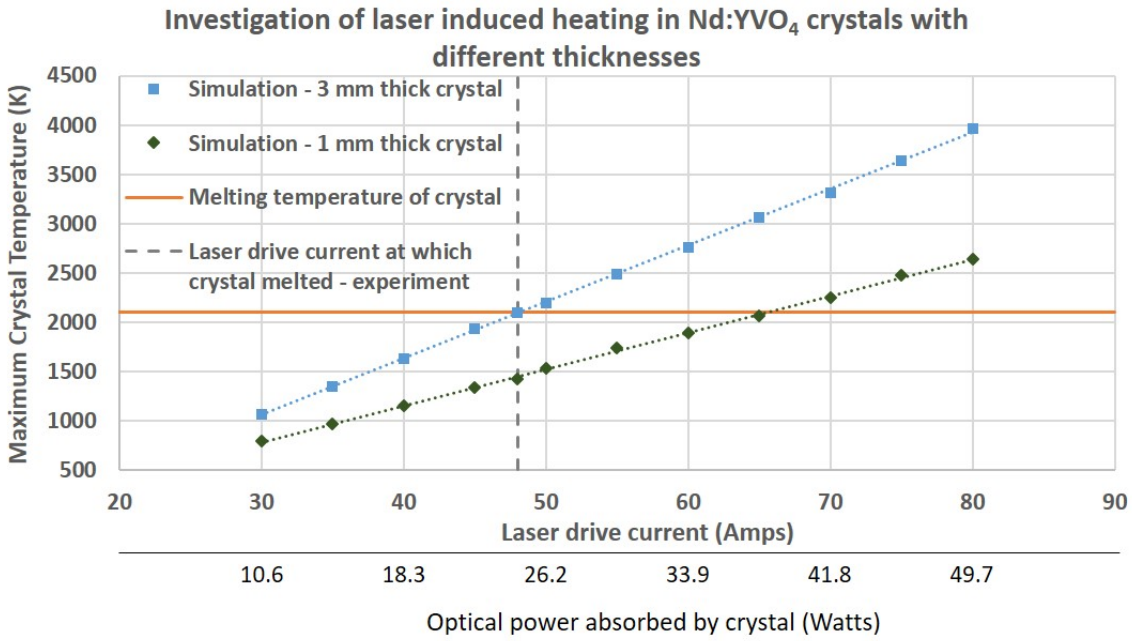

Figure 3.10: Comparison of simulations for laser induced heating of Nd:YVO_4 crystals with different thicknesses, subject to the same optical power loading, Nd doping (3%), and thermal cooling conditions.

be seen that the 1 mm thick crystal survives for a higher laser drive current (65 Amps) without laser induced heat damage, than compared to the 3 mm thick crystal (48 Amps), even though the optical power absorbed by the crystals for a given laser drive current was the same. Thus, reducing the thickness of the laser crystal enables the crystal to be pumped with higher optical powers, thus enabling the crystal to be used for high power Nd:YVO_4 based Diode Pumped Solid State (DPSS) lasers. Such thin disk crystal architectures have minimized the heat

deposition issues in DPSS lasers, as confirmed by the Zemax and LASCAD simulations, and have been widely deployed for high power applications [22].

3.6.2 Generalization of simulations - neodymium doping level

It can be seen from equations 3.3, 3.2 and 3.5 that as the Nd doping % decreases, the absorption length of the incident optical power on the crystal surface increases. Figure 3.11 shows the absorption length for Nd:YVO_4 with different Nd doping percentages, over a temperature ranging from 298 K (room temperature) to 2100 K (melting point of Nd:YVO_4 is 2098 K). It can be seen from Figure 3.11 that

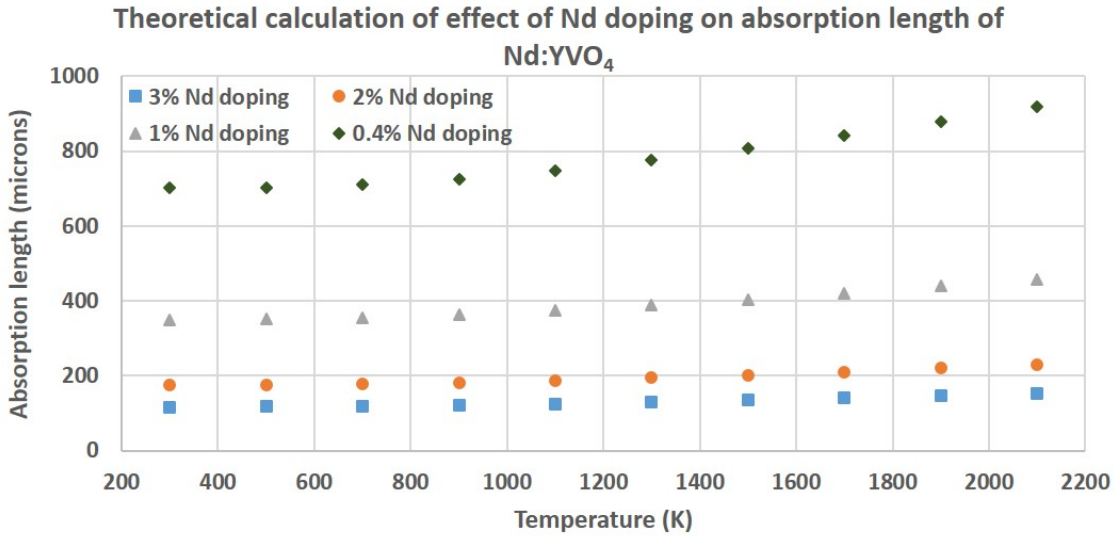

Figure 3.11: Absorption length vs. temperature for Nd:YVO_4 with different levels of Nd doping.

as the Nd doping concentration decreases, the absorption length increases. In addition, the absorption length also increases as the temperature increases, with a greater increase being observed for lower Nd doping concentrations. Since the crystal used in the experiments in this thesis had a 3% Nd doping, which is on the high end of the doping scale for commercially available crystals, simulations were

carried out to study the effect of reducing the Nd doping percentage on the laser induced heating of the crystal. The approximation that by twice the $\frac{1}{e}$ absorption length, all the optical power incident on the crystal surface was absorbed inside the crystal is valid. Thus, a Nd doping of 0.4% was chosen for the simulations, as it was a lower doping concentration that could still absorb all of the incident pump power for a crystal length of 2 mm, over the temperature range from 300 K (room temperature) to 2098 K (melting temperature of Nd:YVO_4). The theoretically calculated transmission information was then entered into Zemax to simulate the crystal, as shown in table 3.6.

Table 3.6: Zemax Transmission Parameters for Nd:YVO_4 Crystal with 0.4% Nd doping

Wavelength	**Transmittance**	**2 × Absorption length**
808 nm	0%	2000 μm

This new crystal with a 0.4% Nd doping was then used in place of the 3% Nd doped crystal in the Zemax setup shown in Figure 3.2, and the simulations for the absorbed flux density were obtained. These Zemax simulations were then imported into LASCAD for thermal analysis. Figure 3.12 shows the LASCAD generated temperature profile for an Nd:YVO_4 crystal with the same parameters as those listed in table 3.5, except for the Nd doping concentration and fractional heat load. The Nd doping was 0.4%, and published literature states that the fractional heat load for Nd:YVO_4 with a Nd doping of 0.4%, in the absence of stimulated emission, is 28% [20]. The crystal modeled in Figure 3.12 was subject to the same optical loading (24.6 W absorbed pump power, corresponds to laser drive current of 48 Amps) and crystal cooling conditions at which the 3% Nd doped crystal first showed signs of laser induced melting. It can be seen that the maximum

temperature reached inside the crystal is much lower than the melting point of Nd:YVO_4 (2098 K), in spite of the fact that 3% Nd doped crystal did not survive at the same heat loading and cooling conditions.

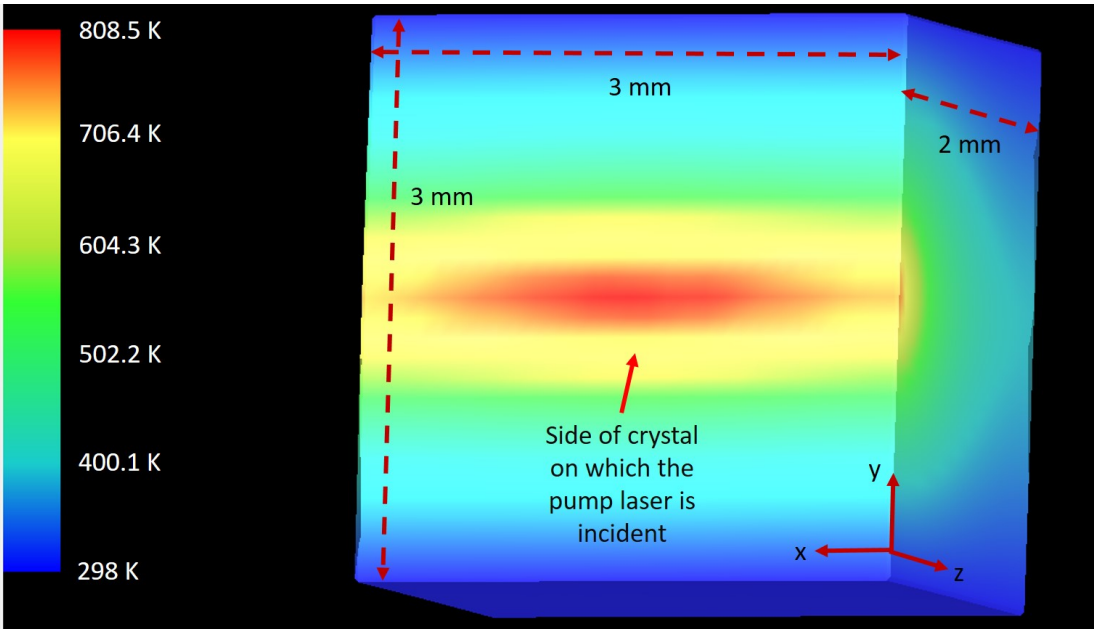

Figure 3.12: LASCAD generated temperature profile of 0.4% Nd doped crystal, subject to the same optical power loading and crystal cooling conditions as those for the crystal with 3% Nd doping modeled in figure 3.6.

Figure 3.13 summarizes the simulation results for the Nd:YVO_4 crystals with a Nd doping of 3% and 0.4%, subject to the same optical power loading by the pump laser diode. In addition, both crystals in the simulations were cooled from top and bottom surfaces, with the temperatures of these surfaces being set to 298 K. It can be seen that the maximum temperature of the 0.4% Nd doped crystal never exceeds the melting temperature of Nd:YVO_4 for the entire range of the laser drive current (30 to 80 Amps), whereas the maximum temperature of the 3% Nd doped crystal exceeded the melting temperature of Nd:YVO_4 at laser drive current of 48 Amps. This happened in spite of the fact that both crystal were subject to the same

optical power loading (for a given laser drive current) and crystal cooling conditions. These simulation results agree with published literature on experimental studies of the effect of doping on the fractional heating load in Nd:YVO_4 [23].

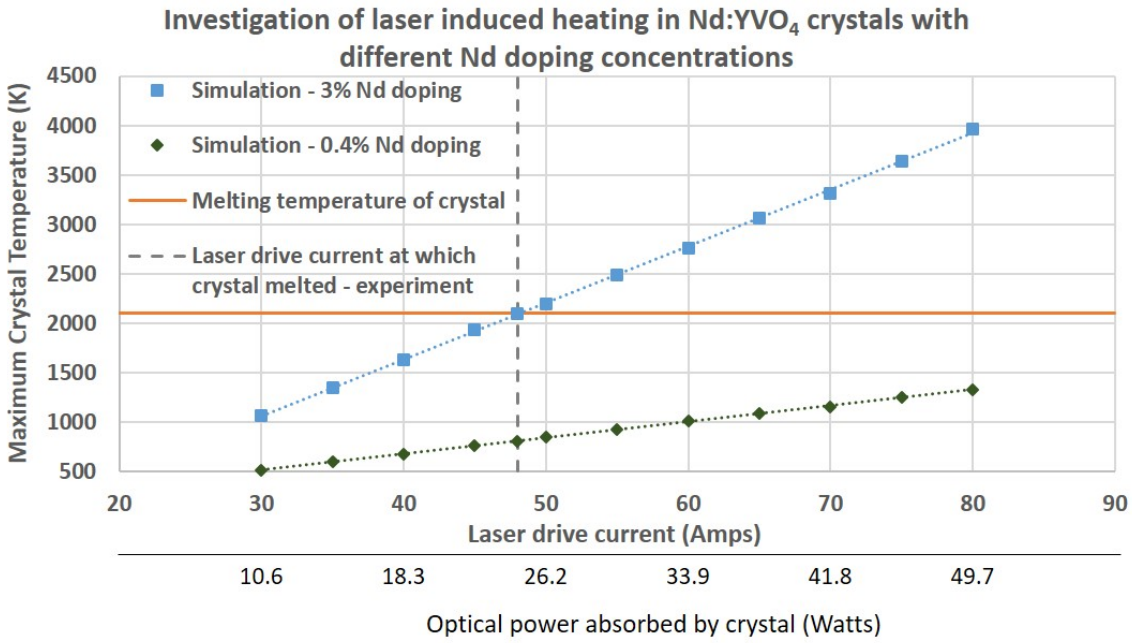

Figure 3.13: Comparison of simulations for laser induced heating of Nd:YVO_4 crystals with different Nd doping, subject to the same optical power loading and thermal cooling conditions.

CHAPTER 4

SIMULATION OF LASER INDUCED THERMAL STRESS FRACTURE IN $Nd:YVO_4$ CRYSTALS

4.1 Thermal stress fracture in $Nd:YVO_4$

A certain fraction of the pump power absorbed by an $Nd:YVO_4$ crystal is converted to heat, as seen in chapter 3. For continuous-wave (cw) pumping, the 3D temperature profile *T(x,y,z)* can be found by solving the steady state differential heat equation, given by [24]

$$\nabla^2 T(x,y,z) + \frac{q(x,y,z)}{k} = 0 \tag{4.1}$$

where *q(x,y,z)* is the heat source that is part of the pump power, and k is the thermal conductivity of the $Nd:YVO_4$ crystal. The thermal boundary conditions for equation 4.1 are defined by the temperature of the coolant flowing though the aluminum blocks between which the crystal is mounted. Equation 4.1 was solved numerically in the LASCAD simulation environment. LASCAD deployed the Finite Element Analysis (FEA) method to obtain the temperature (due to the absorbed pump power) at every node point in the FEA grid, as discussed in chapter 3. The 3D temperature distribution was used to obtain the thermal expansion of the crystal along the x, y, and z axes. This thermal displacement profile was then used to calculate the stress induced in the crystal along the 3 axes. The equilibrium of stresses in cartesian co-ordinates is given by [24]

$$\frac{\partial \sigma_{xx}}{\partial x} + \frac{\partial \sigma_{xy}}{\partial y} + \frac{\partial \sigma_{xz}}{\partial z} = 0 \tag{4.2}$$

$$\frac{\partial \sigma_{yx}}{\partial x} + \frac{\partial \sigma_{yy}}{\partial y} + \frac{\partial \sigma_{yz}}{\partial z} = 0 \tag{4.3}$$

$$\frac{\partial \sigma_{xz}}{\partial x} + \frac{\partial \sigma_{yz}}{\partial y} + \frac{\partial \sigma_{zz}}{\partial z} = 0 \tag{4.4}$$

where the stress components σ_{ii} represent the normal components and σ_{ij}, where i $\neq$ j, represent the shear components. Figure 4.1 shows components of the stress applied to an infinitesimally small cube, which corresponds to a node in the FEA grid [10].

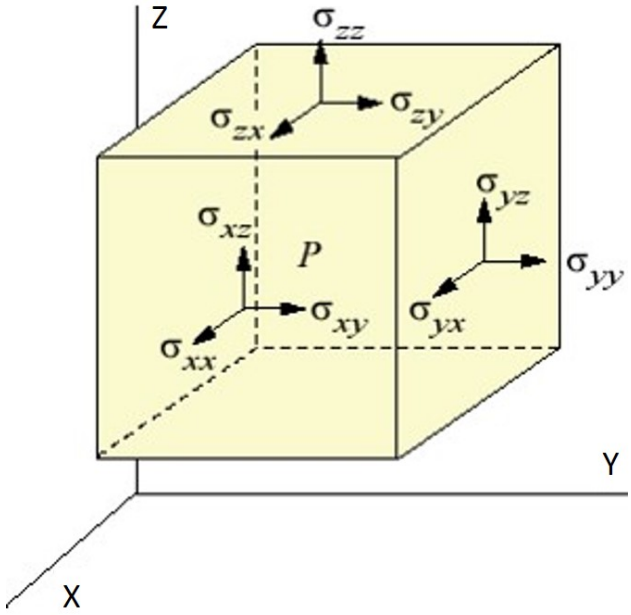

Figure 4.1: Components of stress in three dimensions. Adapted from [10].

The strain-thermal displacement relationships are defined by [24]

$$\varepsilon_{ij} = \frac{1}{2}\left(\frac{\partial u_i}{\partial x_j} + \frac{\partial u_j}{\partial x_i}\right) \tag{4.5}$$

where ε_{ii} are the direct strains in the x, y, and z directions, ε_{ij} with $i \neq j$ represents the shear strains, and u_{ij} represent the displacements due to heating in the x, y and z directions. The stresses, strains, and temperature of the crystal are related by the

generalized Hooke's law, given by [24]

$$\sigma_{xx} = 2\mu\varepsilon_{xx} + \delta_{xx}[\xi e - (3\xi + 2\mu)\alpha T(x, y, z)] \tag{4.6}$$

$$\sigma_{yy} = 2\mu\varepsilon_{yy} + \delta_{yy}[\xi e - (3\xi + 2\mu)\alpha T(x, y, z)] \tag{4.7}$$

$$\sigma_{zz} = 2\mu\varepsilon_{zz} + \delta_{zz}[\xi e - (3\xi + 2\mu)\alpha T(x, y, z)] \tag{4.8}$$

$$\sigma_{xy} = \sigma_{yx} = 2\mu\varepsilon_{xy} \tag{4.9}$$

$$\sigma_{yz} = \sigma_{zy} = 2\mu\varepsilon_{yz} \tag{4.10}$$

$$\sigma_{xz} = \sigma_{zx} = 2\mu\varepsilon_{xz} \tag{4.11}$$

where δ_{ij} is the Kronecker delta function, *T(x,y,z)* is the temperature distribution inside the crystal, e is the sum of the normal strains ($e = \sum \varepsilon_{ii}$), α is the thermal expansion coefficient, ξ and μ are constants related to the Young's modulus E and Poisson ratio v, which are given by [24]

$$\xi = \frac{vE}{(1+v)(1-2v)} \tag{4.12}$$

$$\mu = \frac{E}{2(1+v)} \tag{4.13}$$

Thus, all 9 cartesian components of the stress tensor (σ_{xx}, σ_{yy}, σ_{zz}, σ_{xy}, σ_{yz}, σ_{xz}, σ_{yx}, σ_{zy}, σ_{zx}) are calculated for every node point in the FEA grid by LASCAD's FEA code. The von Mises yield criterion is defined as the critical stress value at which a material starts to yield. The von Mises stress is given by [25]

$$\sigma_{eqv} = \sqrt{\frac{1}{2}[(\sigma_1 - \sigma_2)^2 + (\sigma_2 - \sigma_3)^2 + (\sigma_3 - \sigma_1)^2]} \tag{4.14}$$

where σ_1, σ_2 and σ_3 are the principal stress components obtained by the diagonalization of the stress tensor. Like the temperature, the von Mises stress value was obtained for every node point in the FEA grid. The position and the size

of the maximum von Mises strain in these calculations indicate the pump power and position at which the crystal will fracture. For Nd:YVO_4, the fracture von Mises stress is 53 N/mm^2 [26].

4.2 Simulations and experimental setup

For investigating the laser induced thermal stress in the crystal, the optical system in Zemax and the LASCAD parameters for the crystal are exactly the same as those shown in Figure 3.2 and table 3.5 respectively. The experimental setup used to investigate the laser induced thermal stress in an Nd:YVO_4 crystal is exactly the same as that used to investigate the laser induced heating of the crystal, which is shown in Figure 3.4.

4.3 Comparison of simulations and experimental results

For the experiment, the laser optical output power was varied from 15.5 W to 73.5 W (corresponding to a laser drive current range of 30 to 80 Amps). Thirty amps was the laser drive current by which the laser beam shape was free of the threshold current effects, and a laser drive current of 80 Amps corresponded to the maximum laser drive current in the manufacturer datasheet. As with the experiment, the laser drive current in the simulations was varied from 30 to 80 Amps, to avoid operating the laser near the threshold current (20 Amps), as well as avoid exceeding the maximum laser drive current stated in the manufacturer datasheet (80 Amps). The Zemax data for the absorbed flux density distribution inside the crystal were then imported into LASCAD. The FEA code of LASCAD was used to calculate the 3D temperature profile inside the crystal. LASCAD was then used to calculate the thermal displacements along the x, y, and z axes of the

crystal, using the 3D temperature distribution obtained from the FEA code. Finally, LASCAD was used to calculate the stress profile inside the crystal from the thermal displacement data.

Figure 4.2 shows the results of the LASCAD simulation for the von Mises stress in an Nd:YVO_4 crystal (Nd doping of 3%), subject to an optical power of 10.5 W being coupled into the crystal, which corresponds to a laser drive current of 30 Amps. The top and bottom surfaces of the crystal (y axis) were set to a temperature of 298 K, to simulate the cooling system in the experimental setup. It

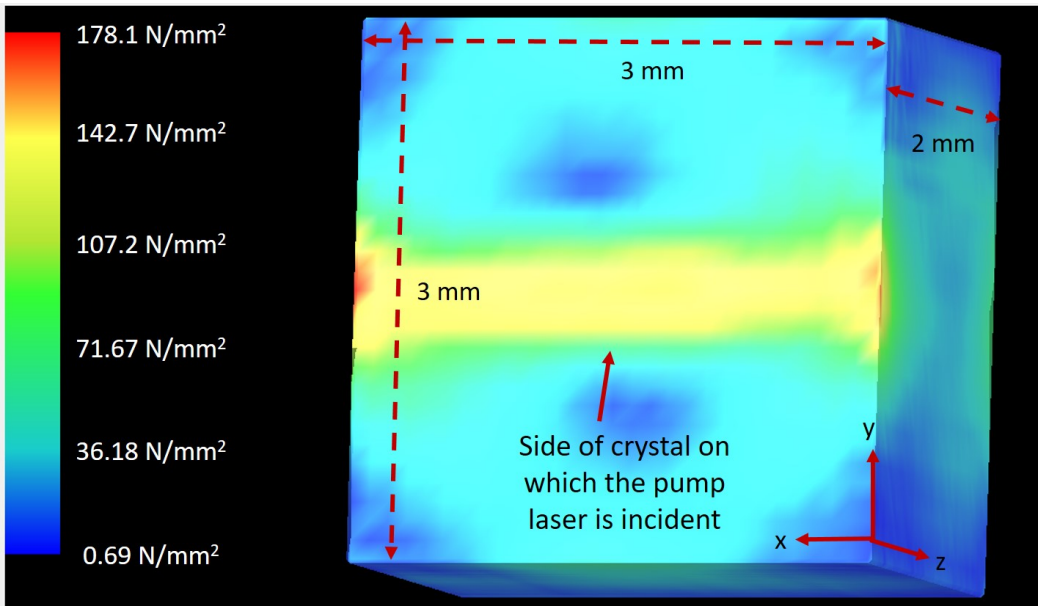

Figure 4.2: LASCAD generated von Mises stress profile of 3% Nd doped crystal, subject to a optical power loading of 10.45 W (corresponds to a laser drive current of 30 Amps).

can be seen from Figure 4.2 that for a laser drive current of 30 Amps, the maximum von Mises stress exceeds the fracture stress limit for Nd:YVO_4 (53 N/mm^2) in the region where the pump laser light was incident. The region of maximum von Mises stress was the same for simulations over the entire optical power loading range, which corresponded to a laser drive current range from 30 to 80 Amps.

Figure 4.3 shows a photograph of the crystal (same as Figure 3.7) used in the experimental measurements of laser induced thermal stress. This crystal was analogous to the Nd:YVO_4 crystal that was simulated in the Zemax and LASCAD environments (Figure 4.2). In addition, the crystal shown in Figure 4.3 was also used in the experiment that was conducted to study the laser induced heat damage in Nd:YVO_4 crystals (experimental setup shown in Figure 3.4). It can be seen that

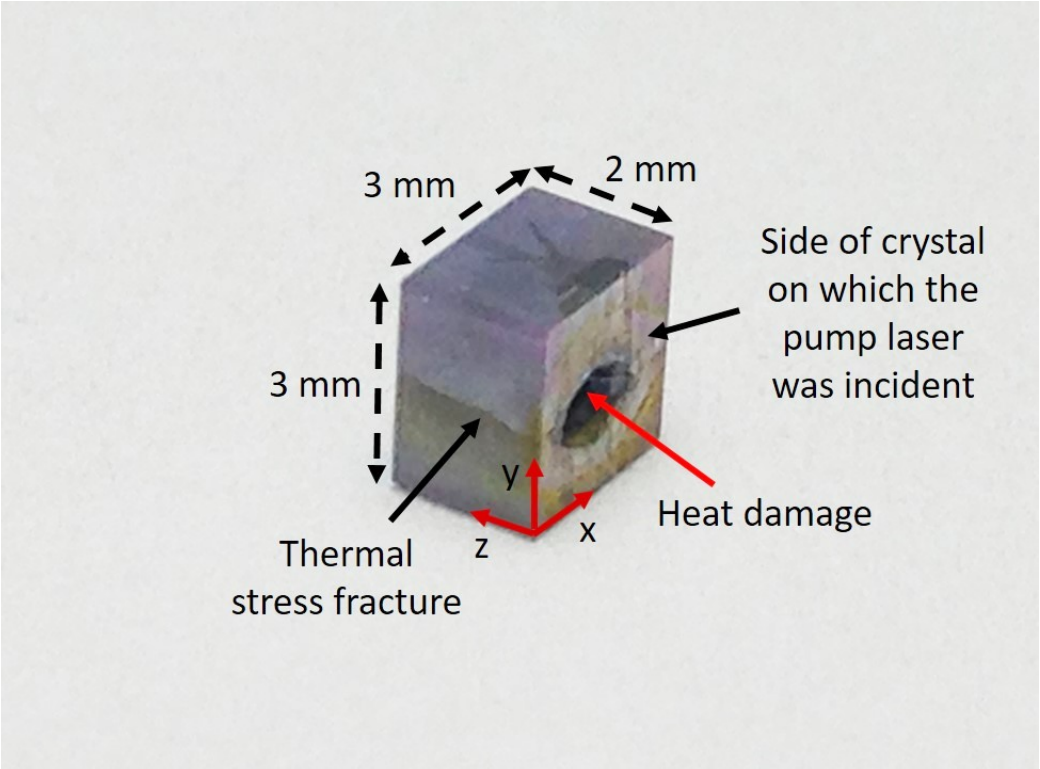

Figure 4.3: Laser induced thermal stress damage in an Nd:YVO_4 crystal with 3% Nd doping.

the fracture line seen in the crystal in Figure 4.3 corresponds to the region of maximum stress in the LASCAD simulation shown in Figure 4.2. In addition, the location of the fracture in the experiment stayed the same over the laser drive current range from 30 to 48 Amps (the crystal started to melt at a laser drive current of 48 Amps). This experimental observation was again consistent with the

simulation results.

Figure 4.4 summarizes the simulation and experimental results for the investigation of laser induced thermal stress fracture in the Nd:YVO_4 crystal (Nd doping of 3%) modeled in Figure 4.2 and shown in Figure 4.3. It can be seen that

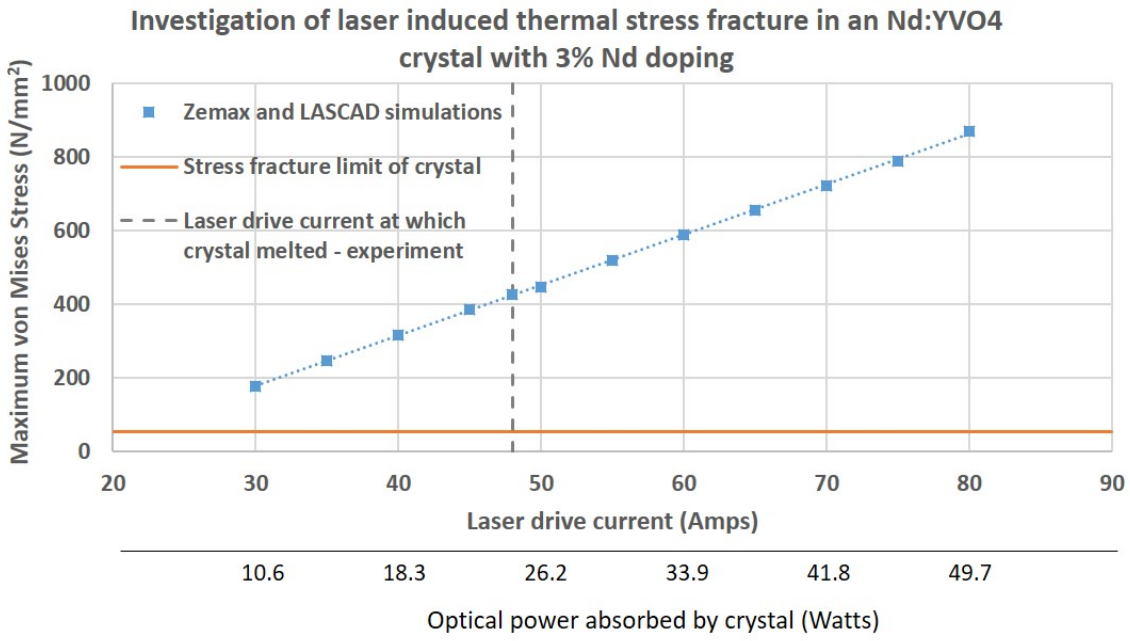

Figure 4.4: Comparison of simulations vs. experimental result for investigation of laser induced heating in an Nd:YVO_4 crystal with 3% Nd doping.

the thermal stress fracture limit has already been exceeded for a laser drive current of 30 Amps, which also happened to be the lowest laser drive current that results in a consistent laser output beam shape. In addition, it is also evident that the laser drive current at which the thermal stress fracture threshold is exceeded ($\leq$ 30 Amps) is lower than the laser drive current at which the crystal started to melt due to laser induced heating (48 Amps). These results are consistent with experimental studies that have shown that the maximum laser output power of end-pumped solid state lasers is limited by the thermal stress fracture of laser crystals [27].

4.3.1 Generalization of simulations - crystal geometry

It was seen in chapter 3 that the crystal geometry influences the temperature distribution inside the crystal, for given optical power loading and crystal cooling conditions. The temperature distribution is a cause of thermal displacements, which in turn results in stress inside the crystal. Thus, the thermal stress inside of a laser crystal is a function of the crystal geometry. Since the crystal used in the experiments in this thesis had a thickness of 3 mm (crystal length along y axis in Figure 4.3), simulations were carried out to study the effect of reducing the thickness on the laser induced thermal stress fracture, for the same crystal cooling system shown in Figure 3.4. A thickness of 1 mm was chosen, which ensured that there were no additional optical power coupling losses, compared to the crystal with a thickness of 3 mm. Table 3.3 shows the Zemax parameters for modeling the crystal with the Nd doping of 3%.

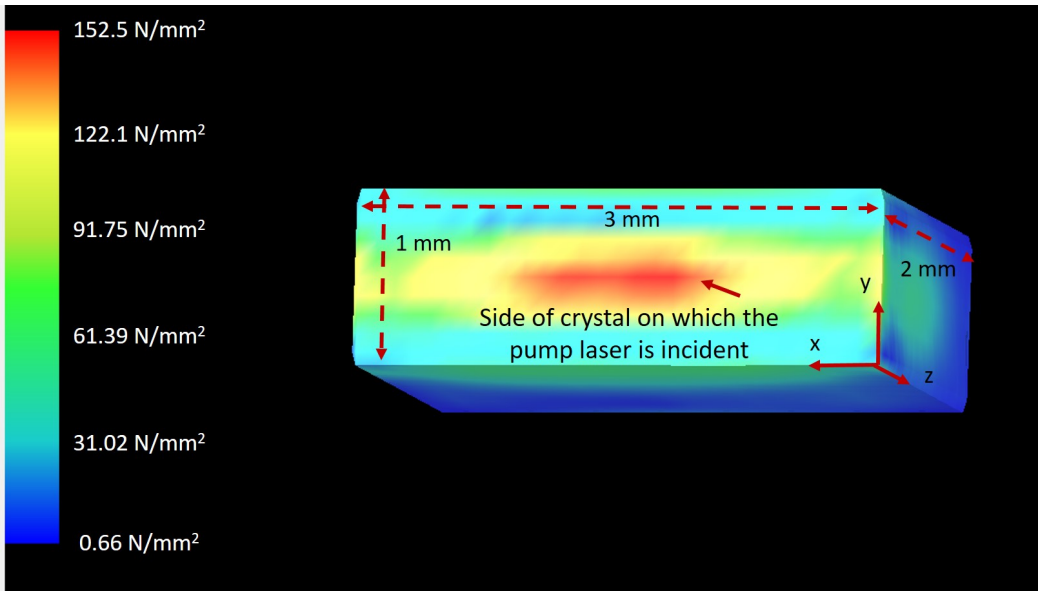

Figure 4.5: LASCAD generated von Mises stress profile of 3% Nd doped crystal, subject to the same optical power loading and crystal cooling conditions as that of the crystal modeled in figure 4.2.

Figure 4.5 shows the LASCAD generated von Mises stress profile of a 1 mm thick Nd:YVO_4 crystal with a Nd doping of 3%, subject to the same optical power loading (10.5 W) and crystal cooling as that of the 3 mm thick crystal modeled in Figure 4.2. It can be seen that the maximum von Mises stress reached inside the 1 mm thick crystal is less than that for the crystal with a thickness of 3 mm, even though both crystals were subjected to the same optical power loading and crystal cooling conditions. The region of maximum von Mises stress was the same for simulations over the entire optical power loading range, which corresponded to a laser drive current range from 30 to 80 Amps.

Figure 4.6 summarizes the simulation results for the Nd:YVO_4 crystals with a thickness of 1 and 3 mm, subject to the same optical power loading by the pump

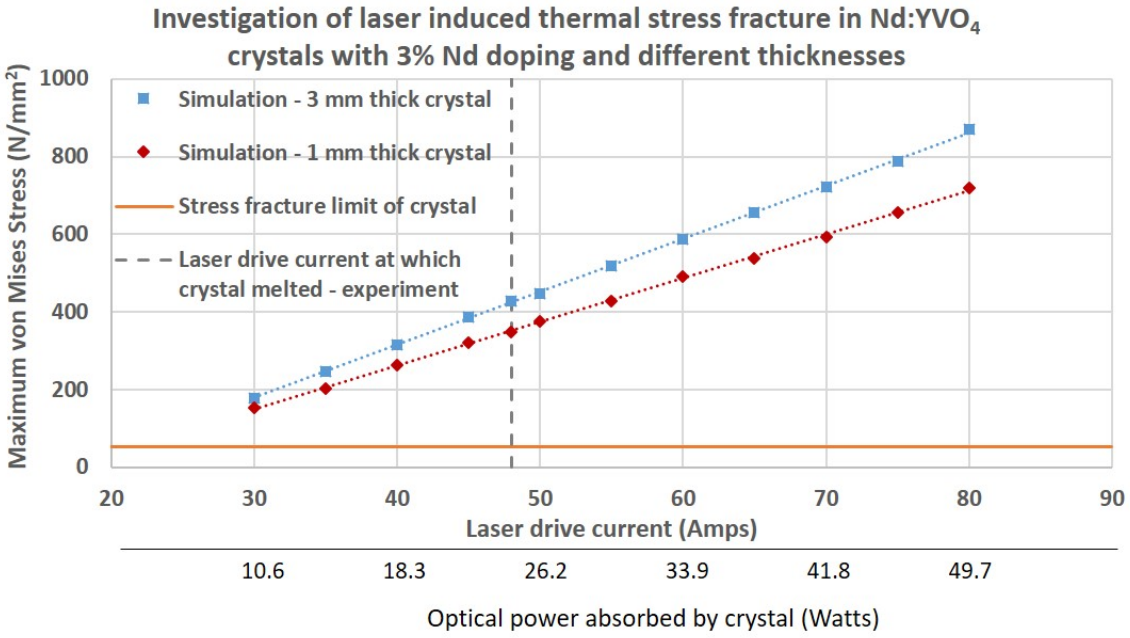

Figure 4.6: Comparison of simulations for laser induced thermal stress fracture in Nd:YVO_4 crystals with different thicknesses, subject to the same optical power loading, Nd doping (3%), and thermal cooling conditions.

laser diode. In addition, both crystals in the simulations were cooled from top and bottom surfaces, with the temperatures of these surfaces being set to 298 K. It can be seen that the 1 mm thick crystal has lower values of the maximum von Mises stress over the entire range of laser drive currents, than compared to the 3 mm thick crystal, even though the optical power absorbed by the crystals for a given laser drive current, as well as the cooling conditions, were exactly the same. Thus, reducing the thickness of the laser crystal decreases the thermal stress inside the crystal, thus increasing the pump power at which thermal stress fracture occurs. This in turn enables the crystal to be pumped with higher optical powers, thus enabling the crystal to be used for high power Nd:YVO_4 based Diode Pumped Solid State (DPSS) lasers [22].

4.3.2 Generalization of simulations - neodymium doping level

Since the crystal used in the experiments in this thesis had a 3% Nd doping, which is on the high end of the doping scale for commercially available crystals, simulations were carried out to study the effect of reducing the Nd doping percentage on the laser induced thermal stress fracture in the crystal. A Nd doping of 0.4% was chosen for the simulations, as it was a lower doping concentration that could still absorb all of the incident pump power for a crystal length of 2 mm, over the temperature range from 300 K (room temperature) to 2098 K (melting temperature of Nd:YVO_4). Table 3.6 shows the Zemax parameters for modeling the crystal with the Nd doping of 0.4%.

This crystal with a 0.4% Nd doping was then used in place of the 3% Nd doped crystal in the Zemax setup shown in Figure 3.2, and the simulations for the absorbed flux density were obtained. These Zemax simulations were then imported into LASCAD for thermal stress analysis. Figure 4.7 shows the LASCAD generated

von Mises stress profile for an Nd:YVO_4 crystal with the same parameters as those listed in table 3.5, except for the Nd doping concentration and fractional heat load. The Nd doping was 0.4%, and published literature states that the fractional heat load for Nd:YVO_4 with a Nd doping of 0.4%, in the absence of stimulated emission, is 28% [20]. The crystal modeled in Figure 4.7 was subject to the same optical loading (10.5 W absorbed pump power, corresponds to a laser drive current of 30 Amps) and crystal cooling conditions as that of the 3% Nd doped crystal modeled in Figure 4.2. It can be seen that the maximum von Mises stress reached inside the crystal is lower than the thermal stress fracture threshold of Nd:YVO_4, in contrast to the fact that the maximum von Mises stress in the 3% Nd doped crystal (modeled in Figure 4.2) exceeded the fracture limit, even though the 3% Nd doped

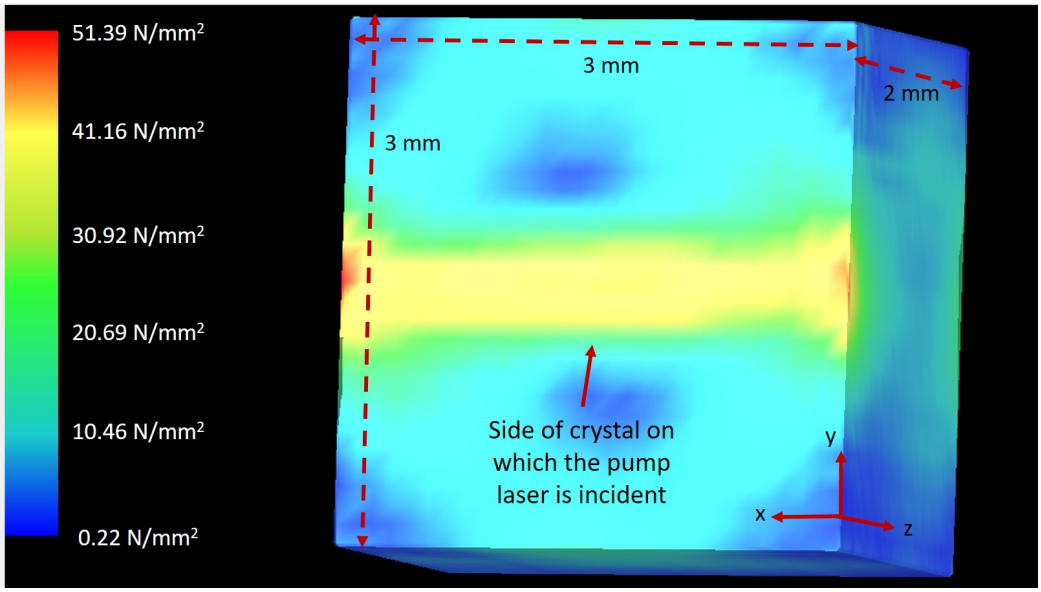

Figure 4.7: LASCAD generated temperature profile of 0.4% Nd doped crystal, subject to the same optical power loading and crystal cooling conditions as those for the crystal with 3% Nd doping modeled in figure 4.2.

crystal was subject to the same optical power loading and crystal cooling conditions as that of the 0.4% Nd doped crystal. In addition, the region of maximum von

Mises stress was the same for simulations over the entire optical power loading range, which corresponded to a laser drive current range from 30 to 80 Amps.

Figure 4.8 shows the LASCAD generated von Mises stress profile of a 1 mm thick Nd:YVO_4 crystal with a Nd doping of 0.4%, subject to the same optical power loading (10.5 W) as that of the 3 mm thick crystal modeled in Figure 4.2. However, in addition to the thin disk architecture, the crystal was also cooled from the left and right surfaces (x axis), as well as at the surface opposite to that on which the pump laser light was incident (along z axis). It can be seen that the maximum von Mises stress reached inside the 1 mm thick crystal is less than that for the crystals modeled in Figures 4.2, 4.5 and 4.7. This is in spite of the fact that all crystal were absorbed the same incident optical power. In addition, the region of maximum von Mises stress was the same for simulations over the entire optical power loading range, which corresponded to a laser drive current range from 30 to 80 Amps.

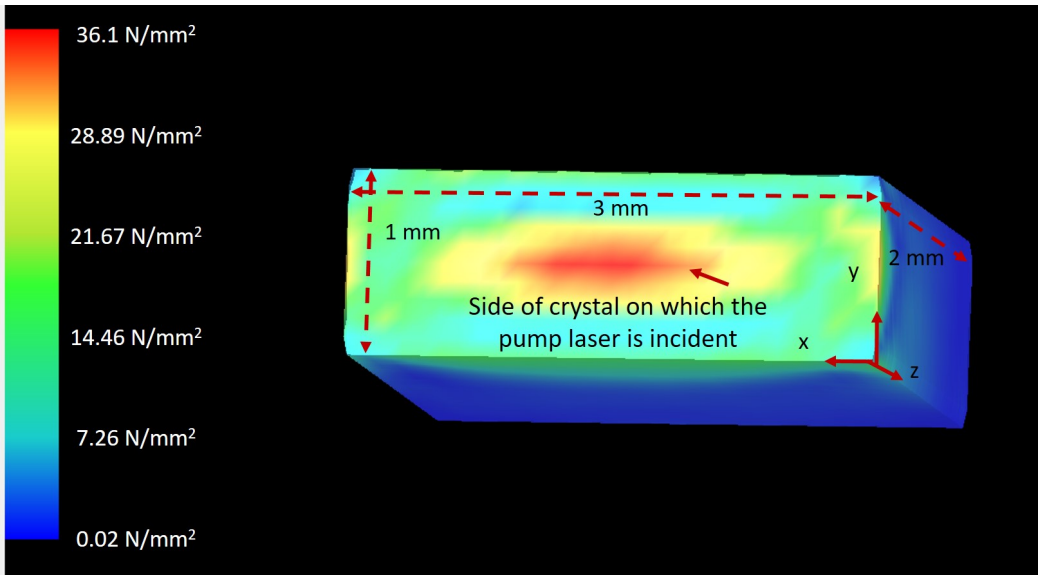

Figure 4.8: LASCAD generated von Mises stress profile of 0.4% Nd doped crystal, subject to the same optical power condition as that of the crystal modeled in figure 4.2.

Figure 4.9 summarizes the simulation results for the Nd:YVO_4 crystals modeled in Figures 4.2, 4.5 and 4.7. These crystals were subject to the same optical power loading by the pump laser diode. The crystals in the simulations in Figures 4.2, 4.5 and 4.7 were cooled from top and bottom surfaces, with the crystal in Figure 4.7 being also cooled from the left, right, and back faces. It can be seen that the maximum von Mises stress of the 0.4% Nd doped [23]. crystals never exceeds

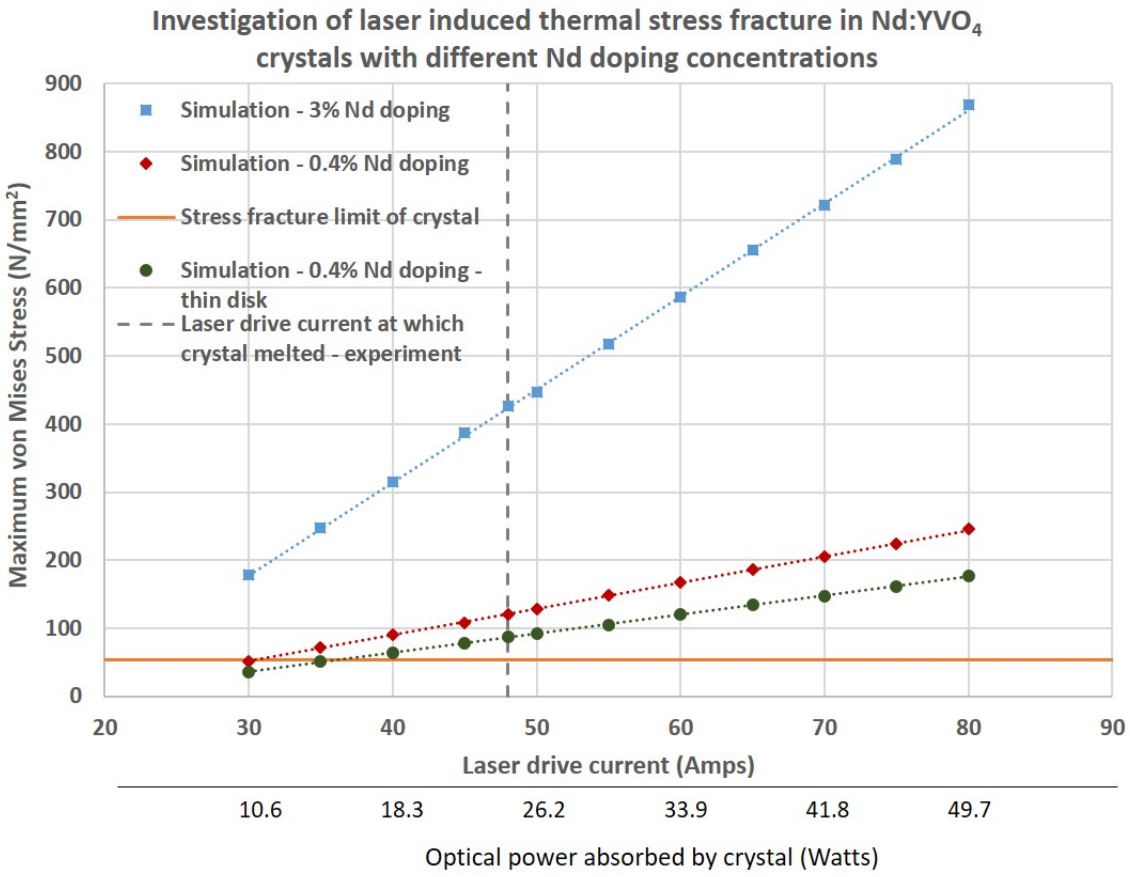

Figure 4.9: Comparison of simulations for laser induced thermal stress in crystals with different Nd doping concentrations, subject to the same optical power loading and thermal cooling conditions.

that of the 3% Nd doped crystal, for the entire range of the laser drive current (30 to 80 Amps). This happened in spite of the fact that all three crystals were subject

to the same optical power loading (for a given laser drive current). In addition, it is also evident that the crystal with a Nd doping of 0.4% and a thin disk architecture has the lowest laser induced thermal stress for the entire range of laser drive current (30 to 80 Amps). These simulation results agree with published literature on experimental studies of the effect of doping on the fractional heating load, and thus thermal stress, in Nd:YVO_4

CHAPTER 5

CONCLUDING REMARKS

5.1 Summary

In this thesis, the thermal damage characteristics (melting and stress fracture) were investigated for a Nd:YVO_4 crystal, with a Nd doping of 3%, subject to optical power loading from the pump laser in the absence of lasing action. The simulation for the laser induced heating and stress in the crystal were compared to the experimental results, and were found to be in agreement. These results were then generalized to Nd:YVO_4 crystals with lower Nd doping concentrations and different geometries. Thus, the effects of the Nd doping and crystal geometry on the laser induced melting and thermal stress fracture of Nd:YVO_4 crystals in the absence of lasing action were also examined.

It was observed in the simulations that in the absence of stimulated emission, reducing the thickness of the crystal (without affecting the efficiency of the optics for coupling the laser light into the crystal) increases the optical power that can be absorbed by the crystal, before the crystal starts to melt due to heat. In addition, the simulations also show that in the absence of stimulated emission, reducing the Nd doping concentration also increases the optical power that can be absorbed by the crystal, before the crystal starts to melt due to heat. Both these simulations were verified by experiments from published literature.

Similarly, it was also found in the simulations that in the absence of stimulated emission, reducing the thickness of the crystal (without affecting the efficiency of the optics for coupling the laser light into the crystal) increases the

optical power that can be absorbed by the crystal, before the crystal fractures due to thermal stress. In addition, the simulations also show that in the absence of stimulated emission, reducing the Nd doping concentration also increases the optical power that can be absorbed by the crystal, before the crystal starts to fracture due to thermal stress. As in the case of the crystal melting, both these simulations were verified by experiments from published literature.

Finally, it was also observed in all the simulations in this thesis that the fracture of the crystal due to thermal stress preceded the melting of the crystal due to heat. This trend was consistent with the experiments carried out in this thesis, as well as published literature.

5.2 Applications

One area where the work in this thesis could be applied is for the thermal tolerancing of high power laser systems operating in rugged environmental conditions. For instance, under extreme vibrations, some of the laser cavity optics could get dislodged, which could reduce the stimulated emission in the crystal. This could sharply increase the fractional heat load in a short duration of time, and cause thermal stress fracture and heat damage in the crystal before the temperature monitoring systems can take corrective action. This could result in more maintenance downtime, as the crystals will have to now be replaced, in addition to realigning the optics. In many cases, the lead times for custom crystal designs can take several weeks, which can lead to financial losses and work shutdowns. Thus, knowledge of the crystal melting and thermal stress failure thresholds in the absence of lasing action can enable better design and engineering practices to thermally tolerance high power lasers. In addition, the results of the simulations can also be

applied to situations where there is stimulated emission in the crystal, provided the absorbed pump power is replaced with the net absorption (absorbed pump power minus power radiated via stimulated emission). Hence, these results are of potential value for the design of high power Nd:YVO_4 lasers.

BIBLIOGRAPHY

[1] Absorption and emission of light. http://www.invocom.et.put.poznan.pl [Online; accessed January 2017].

[2] Lasers. http://electron6.phys.utk.edu/phys250 [Online; accessed January 2017].

[3] Induced laser. http://faculty.kfupm.edu.sa/CHEM/abetar/Research2.htm [Online; accessed November 2016].

[4] T.Y. Fan. Diode-pumped solid state lasers. *The Lincoln Laboratory Journal*, 3(3), 1990.

[5] Hencharl Johan Strauss. *Thermo-optical effects in high-power end-pumped vanadate lasers*. PhD thesis, Stellenbosch University, March 2010.

[6] Walter Koechner and Michael Bass. *Solid-State Lasers: A Graduate Text*. Springer, 2003.

[7] Internal communication - Kyle Arakaki and Pat Maeda - Palo Alto Reasearch Center (A Xerox compamy).

[8] Lens buying guide. https://www.photographytalk.com/lens-buying-guide [Online; accessed October 2016].

[9] Olivier de Weck and Il Yong Kim. Engineering design and rapid prototyping - finite element method. January 2004. http://web.mit.edu/16.810/www/16.810_L4_CAE.pdf.

[10] The definition of stress. http://www.efunda.com/formulae/solid-mechanics/mat-mechanics/stress.cfm [Online; accessed October 2016].

[11] Rudiger Paschotta. Diode-pumped lasers. https://www.rp-photonics.com/diode-pumped-lasers.html [Online; accessed November 2016].

[12] Thomas Hardwell. *Solid State Lasers: Properties and Applications*. Nova Science Publishers, Inc., 2008.

[13] Milton Laikin. *Lens Design*. CRC, 4th edition, 2004.

[14] Radiant Zemax. *Zemax 13 User's Manual*, April 2013.

[15] Christof Pruss, Eugenio Garbusi, and Wolfgang Osten. Testing aspheres. *Optics and Photonics News*, 19, April 2008.

[16] Joseph Geary. *Introduction to Lens Design*. William-Bell,Inc., 2002.

[17] Neodymium: Yttrium orthovanadate. http://www.northropgrumman.com/BusinessVentures/SYNOPTICS/Products/LaserCrystals/Documents/pageDocs/Nd-YVO4.pdf [Online; accessed October 2016].

[18] Alphan Sennaroglu. Experimental determination of fractional thermal loading in an operating diode-pumped nd:yvo4 minilaser at 1064 nm. *Appl. Opt.*, 38(15):3253–3257, May 1999.

[19] Pranab K. Mukhopadhyay, Jogy George, K. Ranganathan, S.K. Sharma, and T.P.S. Nathan. An alternative approach to determine the fractional heat load in solid state laser materials: application to diode-pumped nd:yvo4 laser. *Optics and Laser Technology*, 34(3):253–258, 2002.

[20] J. L. Blows, T. Omatsu, J. Dawes, H. Pask, and M. Tateda. Heat generation in nd:yvo4 with and without laser action. *IEEE Photonics Technology Letters*, 10(12):1727–1729, December 1998.

[21] Finite element analysis. http://www.autodesk.com/solutions/finite-element-analysis [Online; accessed October 2016].

[22] G A Newburgh and M Dubinskii. A diode-pumped nd:yvo 4 thin disk laser with a hetero-composite gain element and dual-face cooling. *Laser Physics Letters*, 10(10):105807, 2013.

[23] Raphy Lavi and Sharone Goldring. Heat generation following direct pumping of nd:yvo4 with and in the absence of stimulated emission. *Advanced Solid-State Photonics*, page WB6, 2006.

[24] Xiaoyuan Peng, Anand Asundi, Yihong Chen, and Zhengjun Xiong. Study of the mechanical properties of nd:yvo4 crystal by use of laser interferometry and finite-element analysis. *Appl. Opt.*, 40(9):1396–1403, Mar 2001.

[25] LASCAD GmbH. *LASCAD 3.6 Manual*, January 2014.

[26] Rudiger Paschotta. *Field Guide to Lasers*, volume FG12. SPIE Press, January 2008.

[27] Y. F. Chen. Design criteria for concentration optimization in scaling diode end-pumped lasers to high powers: influence of thermal fracture. *IEEE Journal of Quantum Electronics*, 35(2):234–239, February 1999.

APPENDIX A

ZEMAX PRESCRIPTIONS FOR LASER DIODE AND ACYLINDRICAL LENS

The lens editor in Zemax allows optical components such as LED's, lasers, lenses, detectors, gratings etc. to be defined in the simulation environment. The following is a list of the Zemax lens editor parameters for the laser and acylindrical lens.

GENERAL LENS DATA:

Glass Catalogs : SCHOTT OHARA NDYVO4

Temperature (C) : 2.00000E+001

Pressure (ATM) : 1.00000E+000

Adjust Index Data To Environment : Off

Primary Wavelength : 0.808 μm

Lens Units : Millimeters

Wavelengths : 1

Units: μm

OBJECT DATA DETAIL:

A.1 Object 1

Object Type : Source Diode (NSC-SDIO)

Reference Object : 0

Inside Of : 0

Layout Rays : 100

Analysis Rays : 200000

Power(Watts) : 73.5

Wavenumber : 0

Color : 0

Astigmatism : 0.05

X-Divergence : 9

X-SuperGauss : 1

Y-Divergence : 0.5

Y-SuperGauss : 1

Number X : 47

Number Y : 1

Delta X : 0.212765

Delta Y : 0

X-Width : 0

X-Sigma : 0

X-Width Hx : 0.01

Y-Width : 0

Y-Sigma : 0

Y-Width Hy : 0.01

A.2 Object 2

Object Type : Toroidal Lens (NSC-TLEN)

Face 0 : Side Faces

Face Is : Object Default

Coating : AR

Scattering : None

Face 1 : Front Face

Face Is : Object Default

Coating : (none)

Scattering : None

Face 2 : Back Face

Face Is : Object Default

Coating : (none)

Scattering : None

Reference Object : 0

Inside Of : 0

XYZ Position : 0 , 0 , 15

Tilt About XYZ : 0 , 0 , 90

Material : S-LAH64 Index at 0.808000 μm = 1.77583782 Radial Height : 9

X Half-Width : 9

Thickness : 6

Rotation R1 : 0

Radius1 : 11.653

Conic1 : -0.541

Coeff1 r^2 : 0

Coeff1 r^4 : -8e-006

Coeff1 r^6 : -7.20658e-008

Coeff1 r^8 : -2.70409e-010

Coeff1 r^{10} : -5.50023e-013

Coeff1 r^{12} : 0

Rotation R2 : 0

Radius2 : 0

Conic2 : 0

Coeff2 r^2 : 0

Coeff2 r^4 : 0

Coeff2 r^6 : 0

Coeff2 r^8 : 0

Coeff2 r^{10} : 0

Coeff2 r^{12} : 0